We are IntechOpen,
the world's leading publisher of
Open Access books
Built by scientists, for scientists

6,900
Open access books available

185,000
International authors and editors

200M
Downloads

154
Countries delivered to

Our authors are among the

TOP 1%
most cited scientists

12.2%
Contributors from top 500 universities

CLARIVATE ANALYTICS
BOOK CITATION INDEX
INDEXED

WEB OF SCIENCE™

Selection of our books indexed in the Book Citation Index
in Web of Science™ Core Collection (BKCI)

Interested in publishing with us?
Contact book.department@intechopen.com

Numbers displayed above are based on latest data collected.
For more information visit www.intechopen.com

Thermal Strain and Magnetization Studies of the Ferromagnetic Heusler Shape Memory Alloys Ni$_2$MnGa and the Effect of Selective Substitution in 3d Elements on the Structural and Magnetic Phase

T. Sakon, H. Nagashio, K. Sasaki, S. Susuga, D. Numakura,
M. Abe, K. Endo, S. Yamashita, H. Nojiri and T. Kanomata

1. Introduction

Ferromagnetic shape memory alloys (FSMAs) have been extensively studied as potential candidates for smart materials. Among FSMAs, Ni$_2$MnGa is the most familiar alloy [1]. It has a cubic $L2_1$ Heusler structure (space group $Fm\overline{3}m$) with the lattice parameter a = 5.825 Å at room temperature, and it orders ferromagnetically at the Curie temperature $T_C \approx 365$ K [2,3]. Upon cooling from room temperature, a martensite transition occurs at the martensite transition temperature $T_M \approx 200$ K. Below T_M, a superstructure forms because of lattice modulation [4,5]. For the Ni–Mn–Ga Heusler alloys, T_M varies from 200 to 330 K by non-stoichiometrically changing the concentration of composite elements.

Several studies on Ni–Mn–Ga alloys address the martensite transition and correlation between magnetism and crystallographic structures [6–18]. Ma *et al*. studied the crystallography of Ni$_{50+x}$Mn$_{25}$Ga$_{25-x}$ alloys (x = 2–11) by powder X-ray diffraction and optical microspectroscopy [7]. In the martensite phase, typical microstructures were observed for x < 7. The martensite variants exhibit configurations typical of self-accommodation arrangements. The TEM image of Ni$_{54}$Mn$_{25}$Ga$_{21}$ indicates that the typical width of a variant is about 1 μm. The interaction between the magnetism and crystallographic rearrangements was discussed in Refs. [1,8,17,18]. The memory strain was observed in single crystal Ni$_2$MnGa and polycrystalline Ni$_{53.6}$Mn$_{27.1}$Ga$_{19.3}$ [10]. As for the magnetism, the magnetic

anisotropy constant K_U in martensite phase is 1.17×10^{-5} J/m^3, which is forth larger than that in austenite phase (0.27×10^{-5} J/m^3) [1]. Manosa *et al.* suggested that the martensitic transition take place in the ferromagnetic phase, and the decrease in magnetization observed at intermediated fields ($0 < B < 1$ T) is due to the strong magnetic anisotropy of the martensite phase in association with the multi-domain structure of the martensite state [8]. Likhachev *et al.* stated that the magnetic driving force responsible for twin boundary motion is practically equal to the magnetic anisotropy constant K_U [17]. The magnetization results indicate that the martensite Ni–Mn–Ga alloys have higher magnetocrystalline anisotropy. This is because lower initial permeability or lower magnetization at low fields than the cubic austenite phase. Furthermore, the magnetization results indicate that the coercivity and saturation field at martensite phase are higher than those of the cubic austenite phase [11–15]. Zhu *et al.* investigated the lattice constant change $\Delta c/c$ of -4.8 % by means of X-ray diffraction study around martensite transition temperature [11]. Chernenko *et al.* also studied about the magnetization and the X- ray powder diffractions and clear changes were found at martensite temperature for both measurements [12]. Murray *et al.* studied the polycrystalline Ni–Mn–Ga alloys [18]. The magnetization step at T_M is also observed and this is a reflection of the magnetic anisotropy in the tetragonal martensite phase. In the martensite phase, strong magnetic anisotropy exists. Then the magnetization that reflects the percentage of the magnetic moments parallel to the magnetic field is smaller than that in the austenite phase where the magnetic anisotropy is not strong in the weak magnetic field. Therefore the magnetization step is observed at T_M. NMR experiments indicate Mn-Mn indirect exchange via the faults in Mn-Ga layers interchange caused by excessive Ga [13]. This result indicates the exchange interaction between Mn-Mn magnetic moments is sensitive with the lattice transformation. Then the magnetism changes from soft magnet in the austenite phase to hard magnet in the martensite phase, which is due to higher magnetic anisotropy.

To use Ni–Mn–Ga alloys as advanced materials for actuators, polycrystalline materials are useful because of their robustness. Moreover, in daily use, magnetic actuators should be used around room temperature (300 K). Therefore, we selected the Ni$_{52}$Mn$_{25}$Ga$_{23}$ alloy, which shows ferromagnetic transition at the Curie temperature T_C, about 360 K, and the martensite transformation occurs around 330 K.

The purpose of this study is to investigate the correlation between magnetism and crystallographic structures as it relates to the martensite transition of Ni$_{52}$Mn$_{12.5}$Fe$_{12.5}$Ga$_{23}$, Ni$_2$Mn$_{0.75}$Cu$_{0.25}$Ga, Ni$_2$MnGa$_{0.88}$Cu$_{0.12}$ and Ni$_{52}$Mn$_{25}$Ga$_{23}$, which undergoes the martensite transition below T_C [6,7]. Especially, we focused on the physical properties in magnetic fields. We performed in this study that by using the polycrystalline samples, it is possible to provide information on the easy axis of the magnetization in the martensite structure with temperature dependent strain measurements under the constant magnetic fields. In this paper, thermal strain, permeability, and magnetization measurements were performed for polycrystalline Ni$_{52}$Mn$_{12.5}$Fe$_{12.5}$Ga$_{23}$, Ni$_2$Mn$_{0.75}$Cu$_{0.25}$Ga, Ni$_2$MnGa$_{0.88}$Cu$_{0.12}$ and Ni$_{52}$Mn$_{25}$Ga$_{23}$ in magnetic fields (B), and magnetic phase diagrams (B–T phase diagram) were constructed. The results of thermal strain in a magnetic field and magnetic-field-induced strain yield information about the twin boundary motion in the fields. From the permeability and

magnetization measurements, the magnetic anisotropy constant K_U can be calculated. The experimental results were compared with those of other Ni–Mn–Ga single crystalline or polycrystalline alloys, and correlations between magnetism and martensite transition were found.

2. Experimental details

The $Ni_{52}Mn_{12.5}Fe_{12.5}Ga_{23}$ and $Ni_2Mn_{0.75}Cu_{0.25}Ga$ alloys were prepared by the arc melting of 99.9 % pure Ni, 99.99 % pure Mn, and Cu, 99.95 % pure Fe, and 6N pure Ga in an argon atmosphere. To obtain homogenized samples, the reaction products were sealed in double evacuated silica tubes, which were annealed at 1123 K for 3 days, and quenched into cold water. The samples obtained for both alloys were polycrystalline.

The $Ni_2MnGa_{0.88}Cu_{0.12}$ alloy was prepared by the arc melting of 99.99 % pure Ni, 99.99 % pure Mn, and Cu, and 99.9999 % pure Ga in an argon atmosphere. To obtain the homogenized sample, the reaction product was sealed in double evacuated silica tubes, which was annealed at 1123 K for 3 days, and quenched into cold water. The obtained sample was polycrystalline. From the x-ray powder diffraction, *14M* (*P2/m*) martensitic structure and *D0₂₂* tetragonal structure were mixed at 298 K [19]. The lattice parameter of tetragonal structure is a = 3.8920 Å and c = 6.5105 Å.

The $Ni_{52}Mn_{25}Ga_{23}$ alloy was prepared by arc melting 99.99% pure Ni, 99.99% pure Mn, and 99.9999% pure Ga in an argon atmosphere. To obtain a homogenized sample, the reaction product was sealed in double-evacuated silica tubes, and then annealed at 1123 K for 3 days and quenched in cold water. The obtained sample was polycrystalline. From x-ray powder diffraction, the *14M* (*P2/m*) martensite structure and the *D0₂₂* tetragonal structure were mixed at 298 K. The lattice parameters of the *14M* structure were a = 4.2634 Å, b = 5.5048 Å, c = 29.5044 Å, and β = 85.863°, and those of the *D0₂₂* structure were a = 3.8925 Å, and c = 6.5117 Å. The size of the sample was 2.0 mm × 2.0 mm × 4.0 mm.

The measurements in this study were performed at atmospheric pressure, P = 0.10 MPa. Thermal strain measurements were performed using strain gauges (Kyowa Dengyo Co., Ltd., Chofu, Japan). Electrical resistivity of the strain gauges was measured by the four-probe method. The relationship between strain, ε, and deviation of electrical resistivity, ΔR, is given by

$$\varepsilon = \frac{1}{K_S} \cdot \frac{\Delta R}{R_0} = \frac{1}{K_S} \cdot \frac{(R - R_0)}{R_0}, \tag{1}$$

where K_S is the gauge factor (K_S = 1.98) and R_0 is the electrical resistivity above T_R. The strain gauge was fixed parallel to the longitudinal axis of the sample.

Thermal strain measurements were performed using a 10 T helium-free cryocooled superconducting magnet at the High Field Laboratory for Superconducting Materials, Institute for Materials Research, Tohoku University. The magnetic field was applied along

the longitudinal axis of the sample. The thermal strain is denoted by the reference strain at the temperature just above T_M.

Magnetization measurements were performed using a Bitter-type water-cooled pulsed magnet (inner bore: 26 mm; total length: 200 mm) at Akita University. The magnetic field was applied along the longitudinal axis of the sample. The values of magnetization were corrected using the values of spontaneous magnetization for 99.99% pure Ni. The magnetic permeability measurements were performed in AC fields with the frequency f = 73 Hz and the maximum field B_{max} = 0.0050 T using an AC wave generator WF 1945B (NF Co., Ltd., Yokohama, Japan) and an audio amp PM17 (Marantz Co. Ltd., Kawasaki, Japan) at Akita University with the same magnet we used for the magnetization measurement, having the compensating high homogeneity magnetic field. AC fields were applied along the longitudinal axis of the sample.

3. Results and discussions

3.1. $Ni_{52}Mn_{12.5}Fe_{12.5}Ga_{23}$ and $Ni_2Mn_{0.75}Cu_{0.25}Ga$

Figure 1 shows the temperature dependence of the linear thermal expansion of $Ni_{52}Mn_{12.5}Fe_{12.5}Ga_{23}$ in static magnetic fields. When cooling from 310 K (Ferro-A phase), the alloy shrinks gradually in zero magnetic fields. Small elongation was observed at 288 K. Then, sudden shrinking occurs below 286 K, which indicates transformation from austenite phase to martensite phase. We define the martensitic transformation temperature T_M as the midpoint of the steep decrease in the cooling measurement. The T_M of this alloy is 284 K. The reason of small elongation at 288 K is considered that $L2_1$ and $14M$ structures coexist each other. Therefore apertures between $L2_1$ and $14M$ structures were originated and small expansion occured. As for $Ni_{2+x}Mn_{1-x}Ga$ alloys, small elongation was observed just above T_M [21]. As shown in reference 20, the phase below T_M is Ferro-M. When heating from 270 K, expansion occurs at about T_R = 288 K, which indicates reverse martensitic transformation. Small elongations just above the temperatures of T_M and T_R were also observed in polycrystalline $Ni_{2+x}Mn_{1-x}Ga$ ($0.16 \leq x \leq 0.20$) [21].

T_M and T_R gradually changed with increasing magnetic fields. The strain at T_M and T_R was about -2.5×10^{-3} (-0.25 %) and was almost the same as that in magnetic fields. Kikuchi $et\ al.$ performed the x-ray diffraction experiments of $Ni_{50+x}Mn_{12.5}Fe_{12.5}Ga_{25-x}$ [20]. The x-ray patterns at room temperature (T = 300 K, austenite phase) for the samples of $0 \leq x \leq 2.0$ were indexed with the $L2_1$ Heusler structure. In the x-ray diffraction pattern at room temperature of the sample with x =2.0, a very weak reflection from a γ phase was observed, where the γ phase has a disordered fcc structure. The lattice parameter a of x = 2.0 was found to be 5.7927 Å [22]. On the other hand, for $x \geq 3.0$, the martensite phase appeared at room temperature. The martensitic structure of x = 3.0 was indexed as a monoclinic structure with $14M$ ($7R$) structure. The lattice parameters of the sample were determined as a = 4.2495 Å, b = 2.7211 Å, c = 29.340 Å, and β = 93.36° at room temperature.
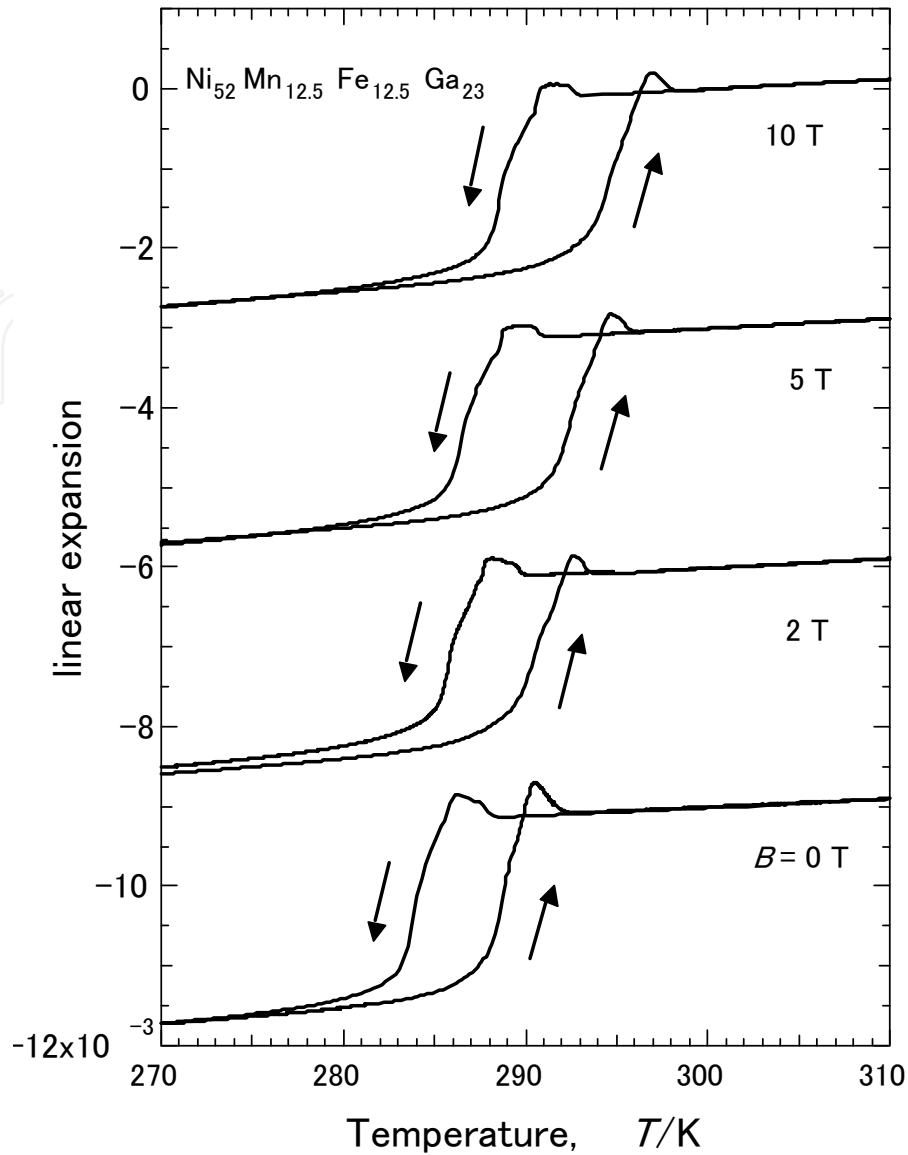
T. Sakon

Figure 1. Temperature dependences of linear thermal expansion of $Ni_{52}Mn_{12.5}Fe_{12.5}Ga_{23}$ in static magnetic fields.

We also estimated the strain of $Ni_{52}Mn_{12.5}Fe_{12.5}Ga_{23}$ ($x = 2.0$) at T_M using the lattice parameter of $x = 2.0$ in the austenite phase and that of $x = 3.0$ in the martensite phase. In the austenite phase, for the $L2_1$ cubic structure, the lattice parameter a was 5.7927 Å [22]. The distance between Mn–Mn atoms was $a/\sqrt{2}$ = 4.0961 Å, and the volume of the unit cell was $V_A = \left(a/\sqrt{2}\right)^3$ = (4.0961)³ = 68.72 Å³. Furthermore, the volume V_M in the martensite phase was estimated and compared with V_A in the same area. In the $14M$ ($7R$) martensite phase, a = 4.2495 Å in the basal plane, is parallel to one of the a axis in the $L2_1$ structure, and is of the same unit. The other axis in the martensite phase corresponds to one of the a axis in the $L2_1$ structure of the Mn–Mn ridge in the basal plane $(\sqrt{2} \times b)$. The c axis is almost normal (β = 93.36°) to the basal plane and the seven Mn–Mn cycles at c = 29.340 Å. Therefore, the volume,

$$V_M = a \times (c/7) \times (\sqrt{2} \times b) \times \sin\beta = 4.2495 \times 4.1914 \times (1.4142 \times 2.7211) \times \sin 93.36° = 68.55 \times 0.9983 = 68.43 \text{ Å}^3. \tag{2}$$

The linear strain of a polycrystal is one-third of the volume strain [24]. Therefore, we estimate the linear strain $\Delta\varepsilon$ as,

$$\Delta\varepsilon = \{(V_M - V_A)/V_A\} \times 1/3 = \{(68.43 - 68.72)/68.72\} \times 1/3 = (-0.29/68.72) \times 1/3 = -0.14 \text{ \%}. \tag{3}$$

This estimated value is approximately comparable to the strain value $\Delta\varepsilon = -0.25$ % of $Ni_{52}Mn_{12.5}Fe_{12.5}Ga_{23}$ obtained from this experimental study.

Figures 2 (a) and (b) show the temperature dependence of magnetic permeability and linear thermal expansion of $Ni_2Mn_{0.75}Cu_{0.25}Ga$ in zero magnetic fields, respectively. When cooling from a high temperature, it shrinks and the permeability increases at about $T_M = 308$ K. The permeability at austenite phase is very low as compared with that at the martensite phase. These results indicate that the region above T_M or T_R is Para-A and the region below T_M or T_R is Ferro-M. When heating from a low temperature, the expansion occurs at about $T_R = 316$ K, which indicates reverse martensitic transformation. The strain at T_M or T_R is about 3.0×10^{-3} (0.30 %). This value is higher than that of $Ni_{52}Mn_{12.5}Fe_{12.5}Ga_{23}$. Kataoka *et al*. studied the x-ray powder diffraction of $Ni_2Mn_{1-x}Cu_xGa_2$ ($0 \le x \le 0.40$) [23]. In the vicinity of martensitic transformation, the strain exhibits complicated behavior; when cooling from 342 K, it shrinks gradually and rapid shrinking occurs at $T_M = 308$ K, subsequently, exhibiting elongation; repetition of small elongation and shrinking was observed between 303 K and 291 K; in addition, it shrinks linearly below 291 K. When heating from 257 K, the repetition of small elongation and shrinking was observed between 307 K and 311 K. Thereafter, it shrinks by 9.0×10^{-4} and exhibits elongation. This sequential phenomenon has been observed in single crystalline $Ni_{2.19}Mn_{0.81}Ga$ [21]. In particular, steep shrinking occurs before elongation due to reverse martensitic transformation during heating. As for polycrystalline $Ni_{2+x}Mn_{1-x}Ga$ ($0.16 \le x \le 0.20$), the shape of the small elongation or small shrinking due to the large change of the strain associated with martensitic transformation is broader than that of the single crystalline alloy. In our study, $Ni_2Mn_{0.75}Cu_{0.25}Ga$ showed steep shrinking before elongation during heating from a low temperature, which is similar to that of single crystalline $Ni_{2.19}Mn_{0.81}Ga$. It is possible that the $Ni_2Mn_{0.75}Cu_{0.25}Ga$ crystal is oriented to some extent.

The x-ray diffraction measurement of $Ni_2Mn_{0.75}Cu_{0.25}Ga$ indicates that cubic *L2₁* phase and the *14M* phase coexist in the martensite phase. The reason for the repetition of small elongation and shrinking in Figure. 2 (b) is supposed to be this complex structure.

Figure 3 shows the temperature dependence of the linear thermal expansion of $Ni_2Mn_{0.75}Cu_{0.25}Ga$ in static magnetic fields. T_M and T_R gradually changed with increasing magnetic fields.

Next, we compared the two samples. The linear thermal coefficients α of $Ni_{52}Mn_{12.5}Fe_{12.5}Ga_{23}$ and $Ni_2Mn_{0.75}Cu_{0.25}Ga$ in zero magnetic fields obtained in this study are shown in Table 1. In the austenite phase, α of $Ni_{52}Mn_{12.5}Fe_{12.5}Ga_{23}$ is much lower than that of $Ni_2Mn_{0.75}Cu_{0.25}Ga$, which means that $Ni_{52}Mn_{12.5}Fe_{12.5}Ga_{23}$ is harder than $Ni_2Mn_{0.75}Cu_{0.25}Ga$. α is higher in the martensite phase than in the austenite phase of $Ni_{52}Mn_{12.5}Fe_{12.5}Ga_{23}$. This is probably due to the *14M* martensitic structure.

(a)

(b)
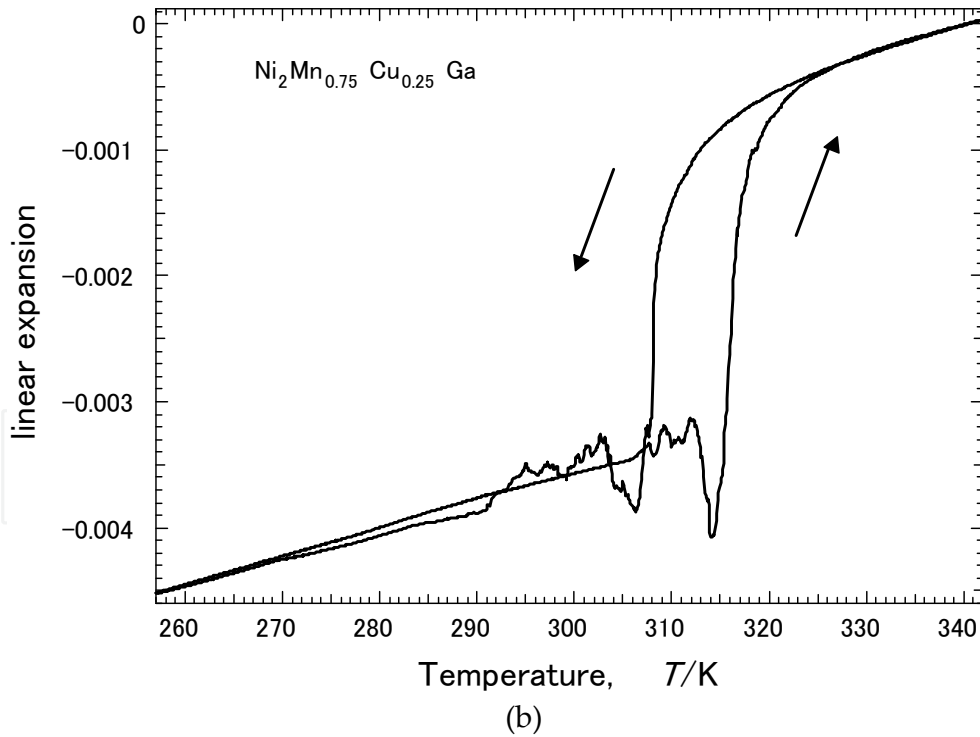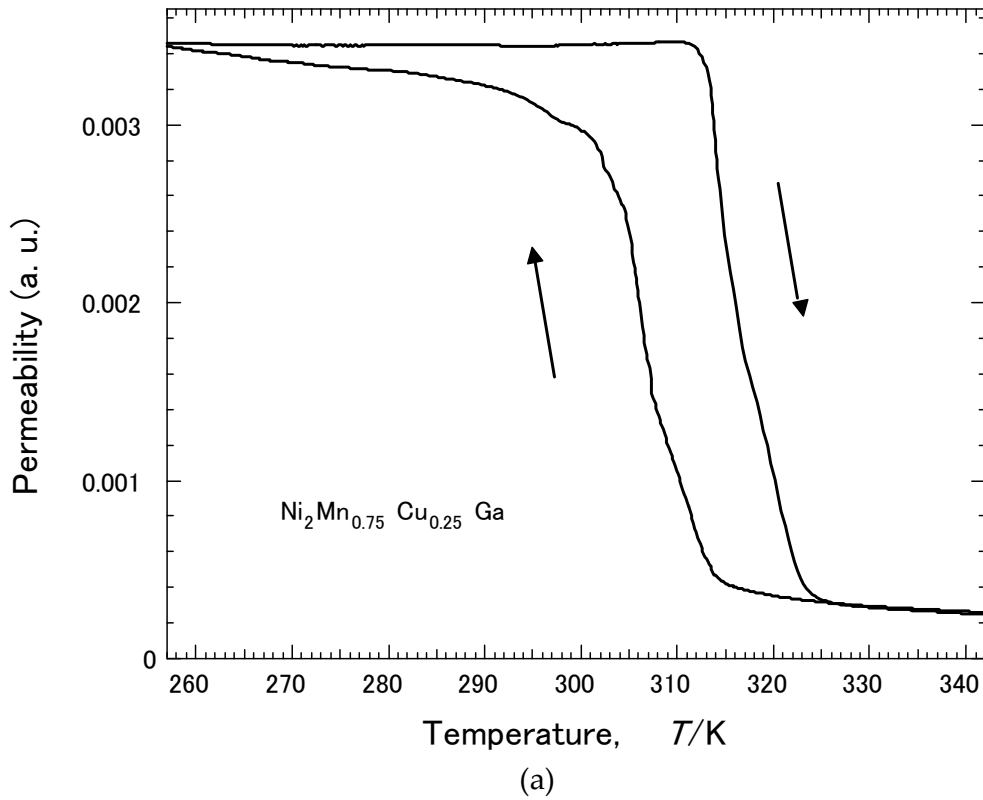
T. Sakon

Figure 2. (a). Temperature dependence of the magnetic permeability μ of Ni₂Mn₀.₇₅Cu₀.₂₅Ga in zero magnetic fields. The magnetic permeability measurement was perforemed in AC fields with f = 73 Hz and B_{max} = 1.0 mT. Zero means the permeability μ = 0. (b) Temperature dependences of linear thermal expansion of Ni₂Mn₀.₇₅Cu₀.₂₅Ga .The strain was defined by the difference from the sample length at 340 K.
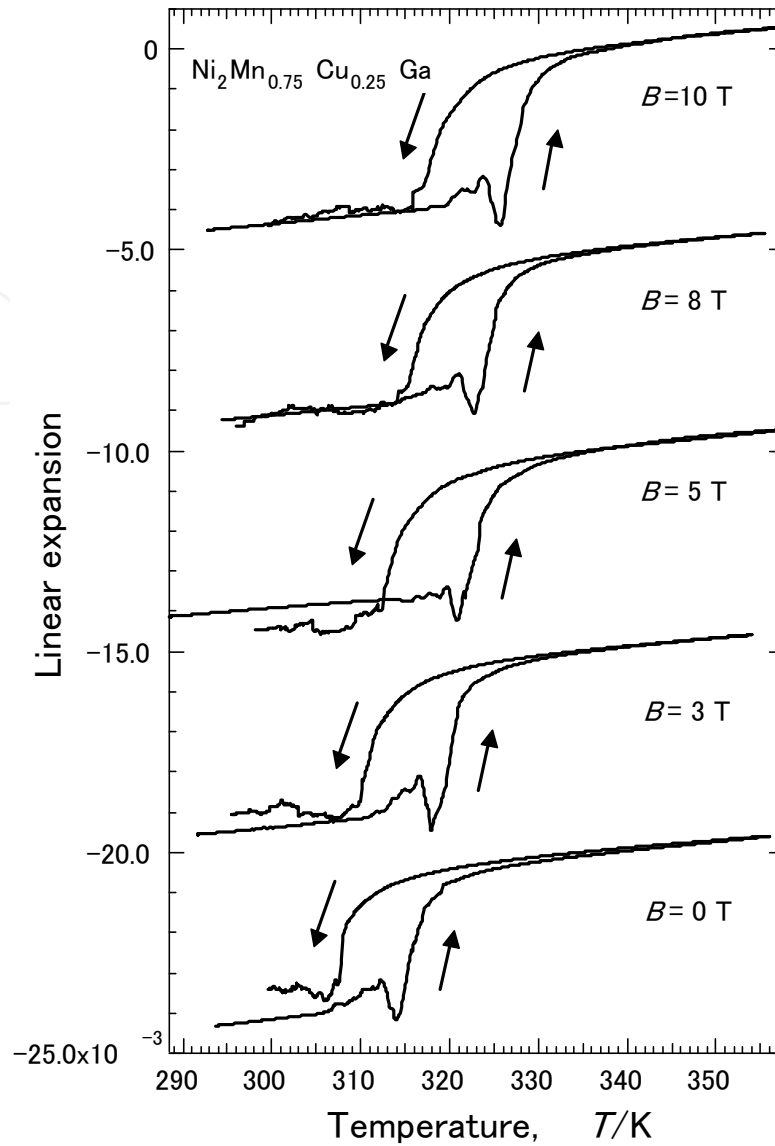
T. Sakon

Figure 3. Temperature dependences of the linear thermal expansion of $Ni_2Mn_{0.75}Cu_{0.25}Ga$ in static magnetic fields.

Figure 4 shows the magnetic phase diagram of the thermal expansion of $Ni_{52}Mn_{12.5}Fe_{12.5}Ga_{23}$ in static magnetic fields. T_M and T_R gradually changed with increasing magnetic fields like $Ni_{2+x}Mn_{1-x}Ga$ alloys. The shifts of T_M and T_R in magnetic fields were estimated as $dT_M/dB \approx 0.5$ K/T and $dT_R/dB \approx 0.5$ K/T, respectively. The shifts of T_M and T_R can be explained by the difference of the magnetization between austenite phase and martensitic phase. Afterwards we discuss about the correlation between magnetization and the shift of T_M.

Figure 5 shows the magnetic phase diagram of the thermal expansion of $Ni_2Mn_{0.75}Cu_{0.25}Ga$ in static magnetic fields. T_M and T_R gradually changed with increasing magnetic fields such as in the $Ni_{2+x}Mn_{1-x}Ga$ or $Ni_{52}Mn_{12.5}Fe_{12.5}Ga_{23}$ alloys. The shifts of T_M and T_R in magnetic fields were estimated as $dT_M/dB \approx 1.2$ K/T and $dT_R/dB \approx 1.1$ K/T, respectively. These ratios are within measurement errors.
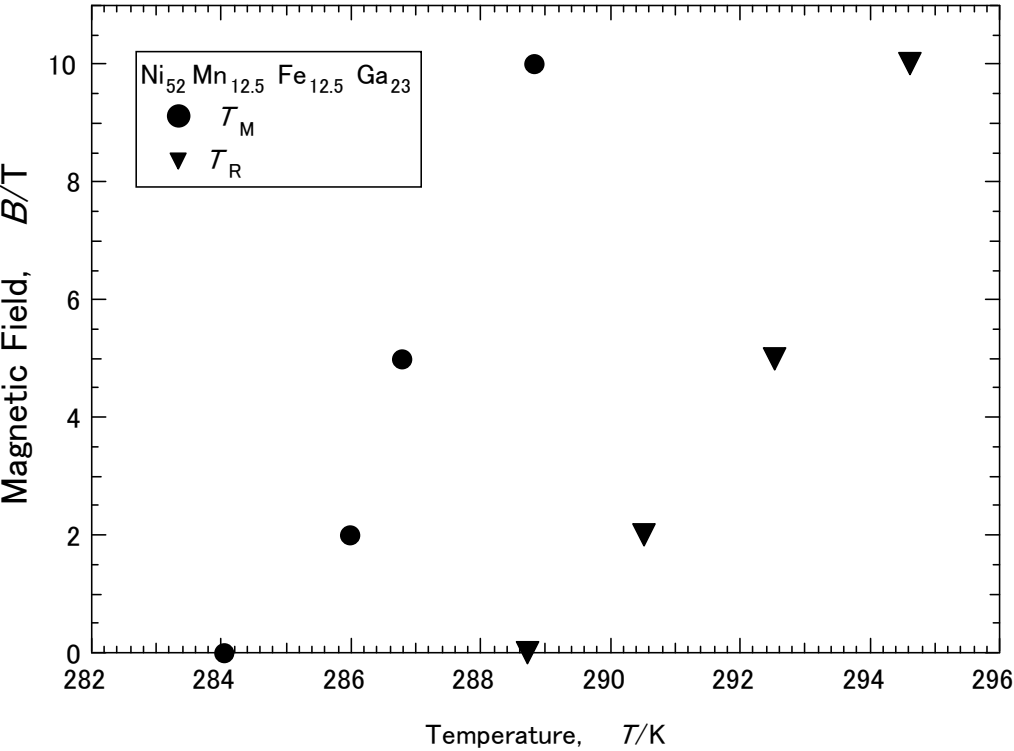
T. Sakon

Figure 4. Magnetic phase diagram of Ni₅₂Mn₁₂.₅Fe₁₂.₅Ga₂₃.
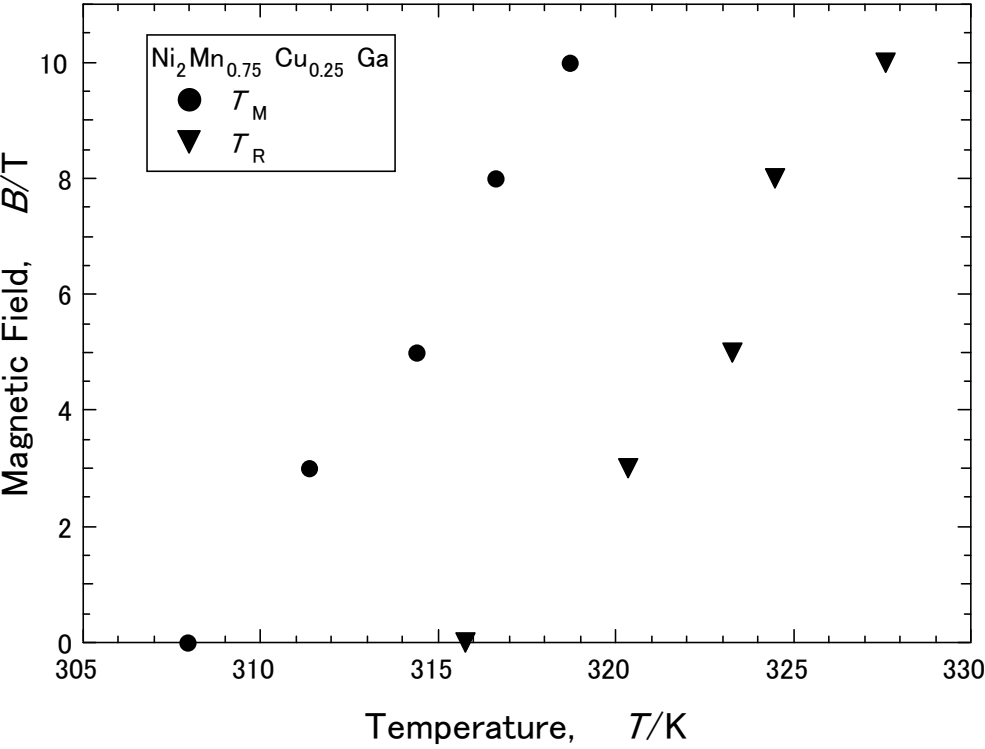
T. Sakon

Figure 5. Magnetic phase diagram of Ni₂Mn₀.₇₅Cu₀.₂₅Ga.

sample	M_M	M_A	$(M_M - M_A)/M_M$	dT_M/dB(K/T)	remarks
Ni$_2$MnGa	90 J/$\mu_0$kgT at 180 K (*1) Ferro	80 J/$\mu_0$kgT at 220 K (*1) Ferro	0.11	0.20 (*2) 0.40 ± 0.25 (*3)	*1 ref. 2 *2 ref. 35 *3 ref. 36
Ni$_{2.19}$Mn$_{0.81}$Ga	2.0 (a.u.) (*4) at 300 K Ferro	0 (a.u.) (*4) at 350 K Para	1.0	1.0 (*4)	*4 ref. 38
Ni$_{52}$Mn$_{12.5}$Fe$_{12.5}$Ga$_{23}$	63.1 J/$\mu_0$kgT at 250 K Ferro	52.7 J/$\mu_0$kgT at 300 K Ferro	0.16	0.5	ref. 27
Ni$_2$Mn$_{0.75}$Cu$_{0.25}$Ga	42.4 J/$\mu_0$kgT at 300 K Ferro	0 J/$\mu_0$kgT at 307 K Para	1.0	1.2	ref. 27
Ni$_2$MnGa$_{0.88}$Cu$_{0.12}$	37.3 J/$\mu_0$kgT at 330 K Ferro	0 J/$\mu_0$kgT at 340 K Para	1.0	1.3	ref. 39
Ni$_{52}$Mn$_{25}$Ga$_{23}$	42.2 J/$\mu_0$kgT at 333 K Ferro	34.2 J/$\mu_0$kgT at 335 K Ferro	0.19	0.43	this work

Table 1. Spontaneous magnetization and dT_M/dB of Ni$_{2+x}$Mn$_{1-x}$Ga, Ni$_{52}$Mn$_{12.5}$Fe$_{12.5}$Ga$_{23}$, Ni$_2$Mn$_{0.75}$Cu$_{0.25}$Ga, Ni$_2$MnGa$_{0.88}$Cu$_{0.12}$, and Ni$_{52}$Mn$_{25}$Ga$_{23}$. M_M and M_A indicate the spontaneous magnetizations in martensite phase and austenite phase, respectively. Ferro and Para mean the ferromagnetic and the paramagnetic phases, respectively.

The magnetic phase diagrams constructed from the thermal expansion measurements of this study are shown in Figures 4 and 5.

Figure 6 (a) shows the magnetization of Ni$_{52}$Mn$_{12.5}$Fe$_{12.5}$Ga$_{23}$ in a pulsed magnetic field. Below 250 K in the Ferro-M state, the M-B curves resemble each other, and this is consistent with the results in reference 7. In the Ferro-A state, the magnetization at 300 K is lower than that in the Ferro-M state. Figure. 6 (b) shows the high-field magnetization in a pulsed magnetic field. At 90 K, steep increase in magnetization occurs when magnetic field is applied. Above 2 T, the magnetization increases gradually. The magnetization at 300 K, which is above T_M and T_R, is also ferromagnetic. The magnetization above 5 T is almost flat. This property is quite different from that at T = 90 K. The magnetism of the austenite phase appears to be similar to a localized ferromagnetic state, because the magnetization value is constant in high magnetic fields.
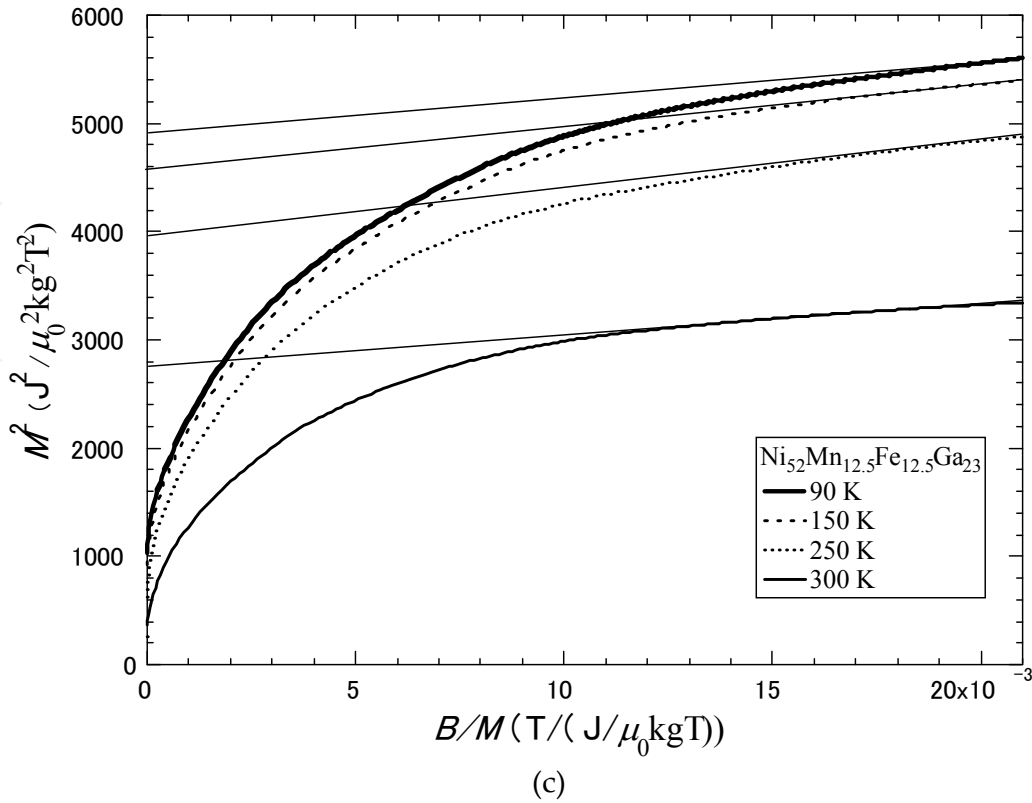
Figure 6. (c) shows an Arrott plot, i.e., M^2 vs B/M, of the magnetization of Ni$_{52}$Mn$_{12.5}$Fe$_{12.5}$Ga$_{23}$. The spontaneous magnetizations at 90 K and 250 K in a Ferro-M state are 70.1 J/$\mu_0$kgT and 63.1 J/$\mu_0$kgT, respectively. The spontaneous magnetization at 300 K in a Ferro-A state is 52.7 J/$\mu_0$kgT.

(a)

(b)

(c)
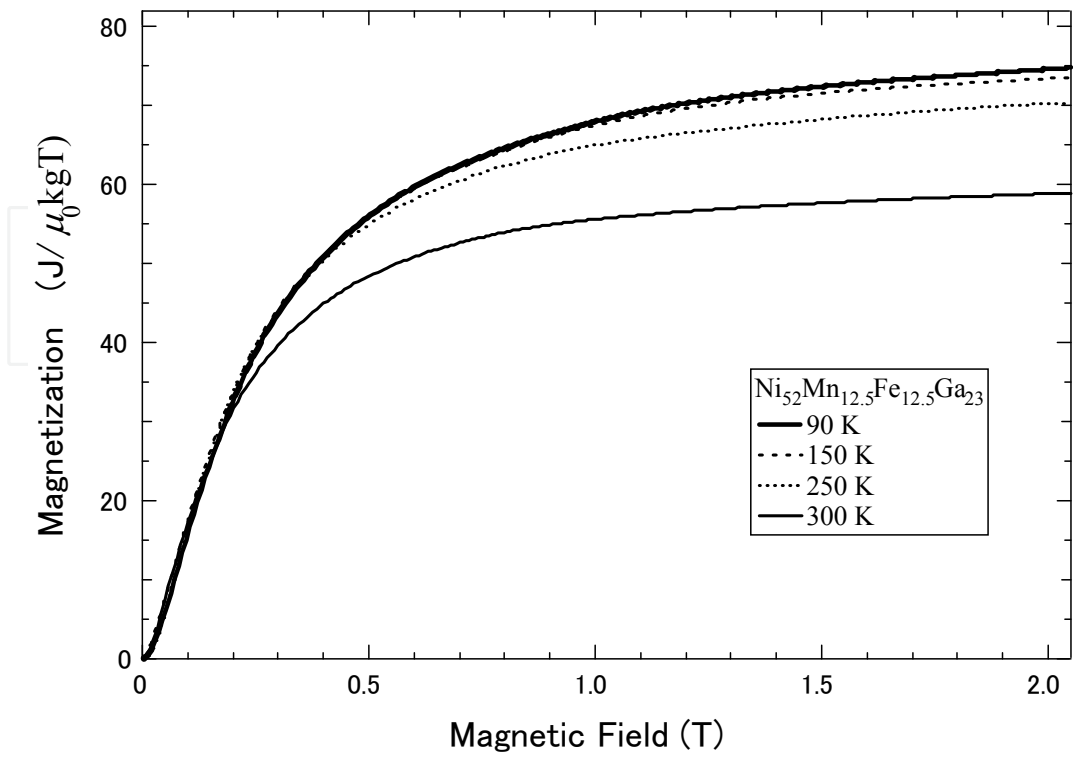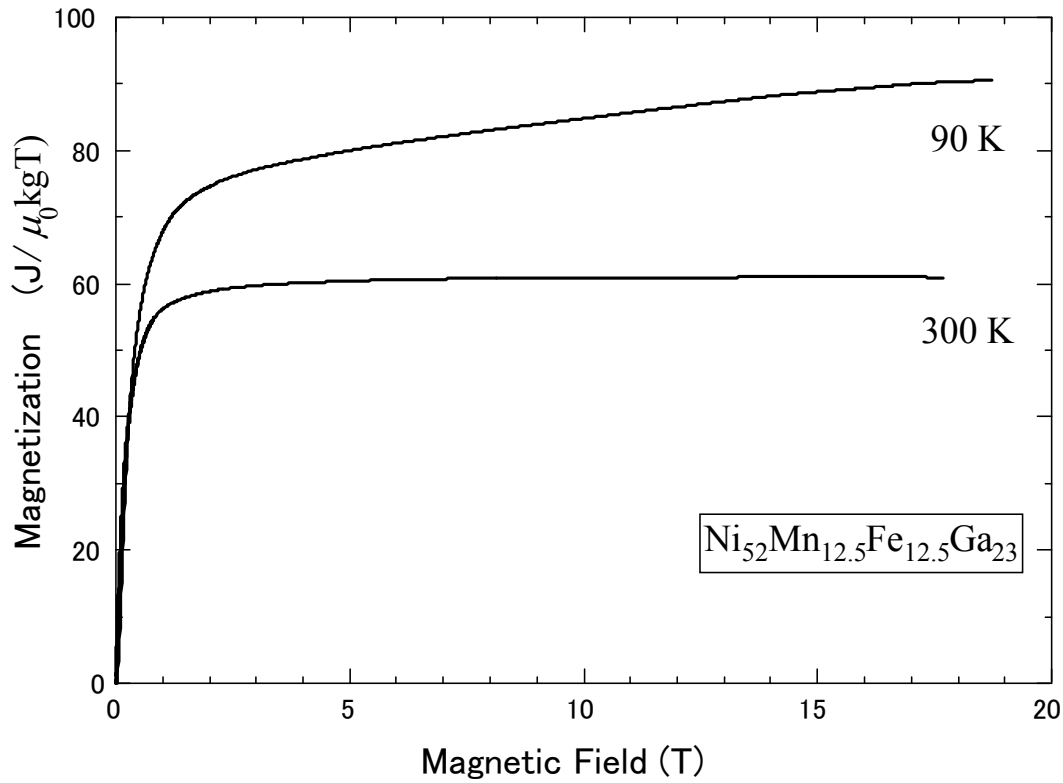
T. Sakon

Figure 6. (a) Magnetization of $Ni_{52}Mn_{12.5}Fe_{12.5}Ga_{23}$ in a pulsed magnetic field up to 2 T. (b) High field magnetization of $Ni_{52}Mn_{12.5}Fe_{12.5}Ga_{23}$ using a pulsed magnet. (c) Arott plot of the magnetization of $Ni_{52}Mn_{12.5}Fe_{12.5}Ga_{23}$. Fine straight lines are extrapolated lines.

Figures 7 (a) and (b) show the magnetization of $Ni_2Mn_{0.75}Cu_{0.25}Ga$ in a pulsed magnetic field. These measurements were performed after zero-field cooling processes at 323 K in the austenite phase. Below T_M, the magnetization shows ferromagnetic properties, whereas above T_M it exhibits paramagnetic properties. This is consistent with the permeability result shown in Figure. 2. Below T_M, for instance, at 300 K, a steep increase occurred around zero fields and a spin-flop like behavior was shown below 0.06 T. Usually, magnetic alloys such as $FeCl_3$ show spin-flop behavior, and a linear extrapolation line at the canted magnetic moments phase crosses the origin point of the coordinate axis in the M-B graph. However, in Figure 7 (a), the M-B graph shows that the linear extrapolation line at the canted magnetic moments phase did not cross the origin point at 300 K. It is possible that steep increase just above the zero fields was due to the localized magnetic moments on the Mn atoms, for example, 3.8–4.2 μ_B/Mn atom which was obtained by the neutron scattering experiments of $Ni_{2+x}Mn_{1-x}Ga$ alloys [2, 24-25]. The magnetic moments on Ni atoms are considerably low, such as 0.2 μ_B/Ni atom for $Ni_{2+x}Mn_{1-x}Ga$ alloys [2, 24-25], and therefore, it is possible that the Ni moments that were arranged in a canted-like formation get ordered by the mutual correlations between external magnetic fields and internal magnetic fields due to the Mn moments.
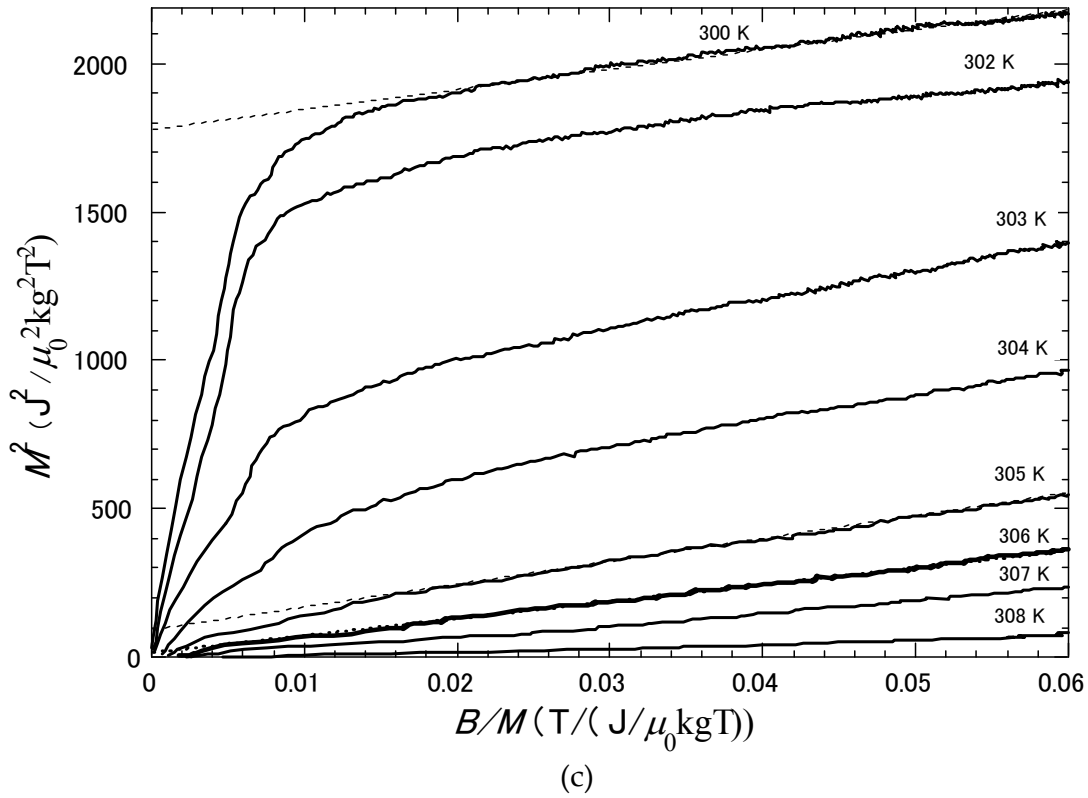
(a)

(b)

(c)
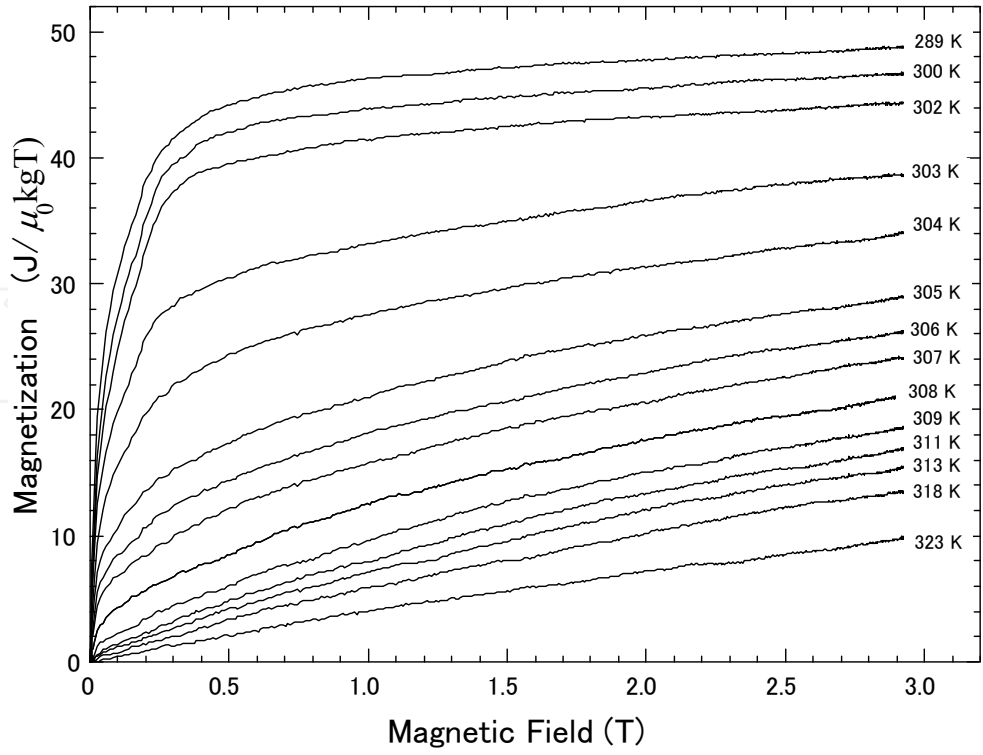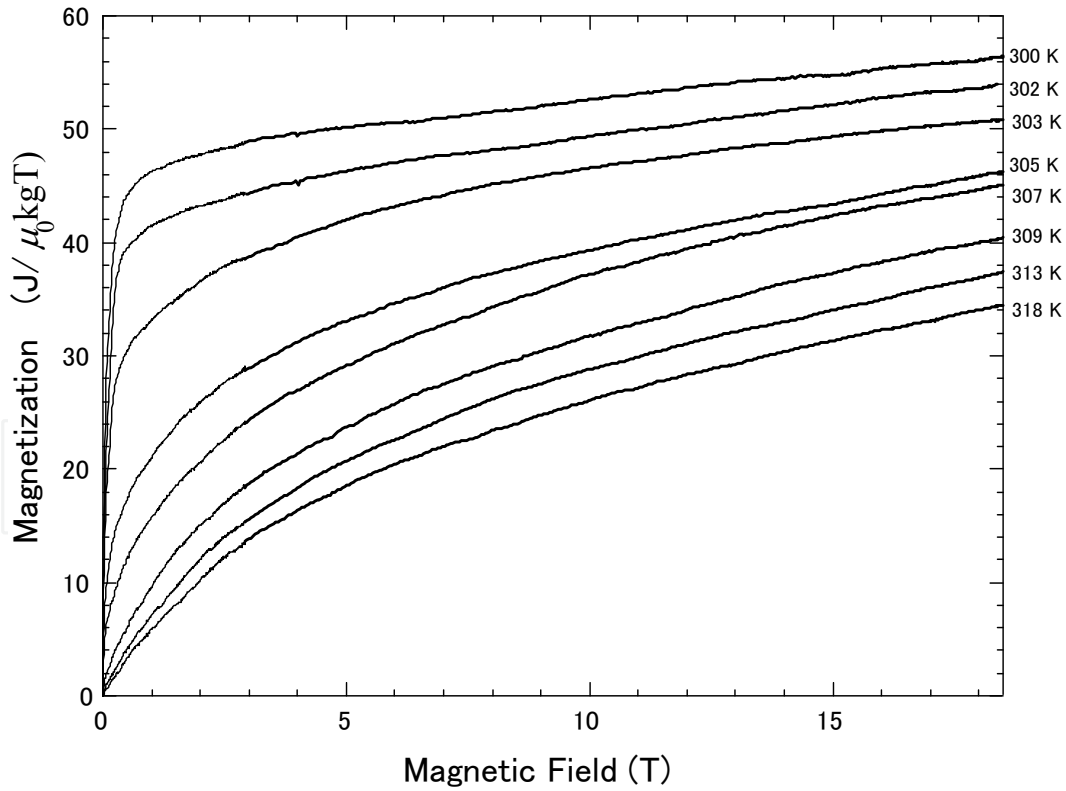
T. Sakon

Figure 7. 7 (a) Magnetization of Ni2Mn0.75Cu0.25Ga in a pulsed magnetic field up to 3 T. (b) High field magnetization of Ni2Mn0.75Cu0.25Ga using a pulsed magnet. (c) Arott plot of the magnetization of Ni2Mn0.75Cu0.25Ga. Dotted lines at 305 K and 306 K are extrapolated linear lines.

Figure 7 (c) shows the Arrott plot of Ni2Mn0.75Cu0.25Ga. The spontaneous magnetization at 300 K in a Ferro-M state is 42.4 J/$\mu_0$kgT. The obtained T_C of the martensite phase is 307 K, which is almost the same as T_M = 308 K and this is consistent with the x-T phase diagram of Ni2Mn1-xCuxGa, which is obtained experimental and theoretical calculations [23].

3.2. Ni2MnGa0.88Cu0.12

Figure 8 shows the temperature dependence of magnetic permeability. When heating from 310 K, the signal gradually increased. A slightly peak was observed at 338 K and a sudden decrease occurred around 342 K. When cooling from a high temperature, the permeability shows a sharp peak at about 337 K. A dip was observed around 324 K. Figure 9 shows the linear thermal expansion. When heating from 305 K, slight expansion was observed at zero magnetic fields. Around 343 K, a sharp expansion was observed. Considering the results of a previous study [19], this is due to the reverse martensitic transition and T_R = 343 K, which is defined as the midpoint temperature of the transition. When cooling from 360 K, a sudden shrinking was observed at 336 K. Considering the lattice structure, the martensitic transition temperature T_M is 336 K. When cooling below 336 K, the linear expansion shows a dip and below 320 K, the value of linear expansion is nearly constant. Mentioned above, the permeability measurement also shows a dip between 336 K and 320 K. As for the

permeability of pure Fe, a large peak was observed just below $T_C = 1040$ K [26]. The half width of the peak ΔT is about 100 K and the ratio $\Delta T / T_C = 0.095$. Meanwhile, the half width of the peak ΔT of the permeability of $Ni_2MnGa_{0.88}Cu_{0.12}$ is about 4 K and $T_C = 345$ K. Then the ratio $\Delta T / T_C = 0.012$, which indicates the increase of the permeability of $Ni_2MnGa_{0.88}Cu_{0.12}$ occurs within a narrower temperature range than that of pure Fe. Concerning the permeability and linear expansion results, dips and drastic changes, the magnetism and the lattice affects one another. The permeability of the austenite phase is very low as compared with that at the martensite phase. The results of the permeability and the linear expansion measurements indicate that the region above T_M is a paramagnetic austenite phase (Para-A) and the region below T_M is a ferromagnetic martensite phase (Ferro-M).
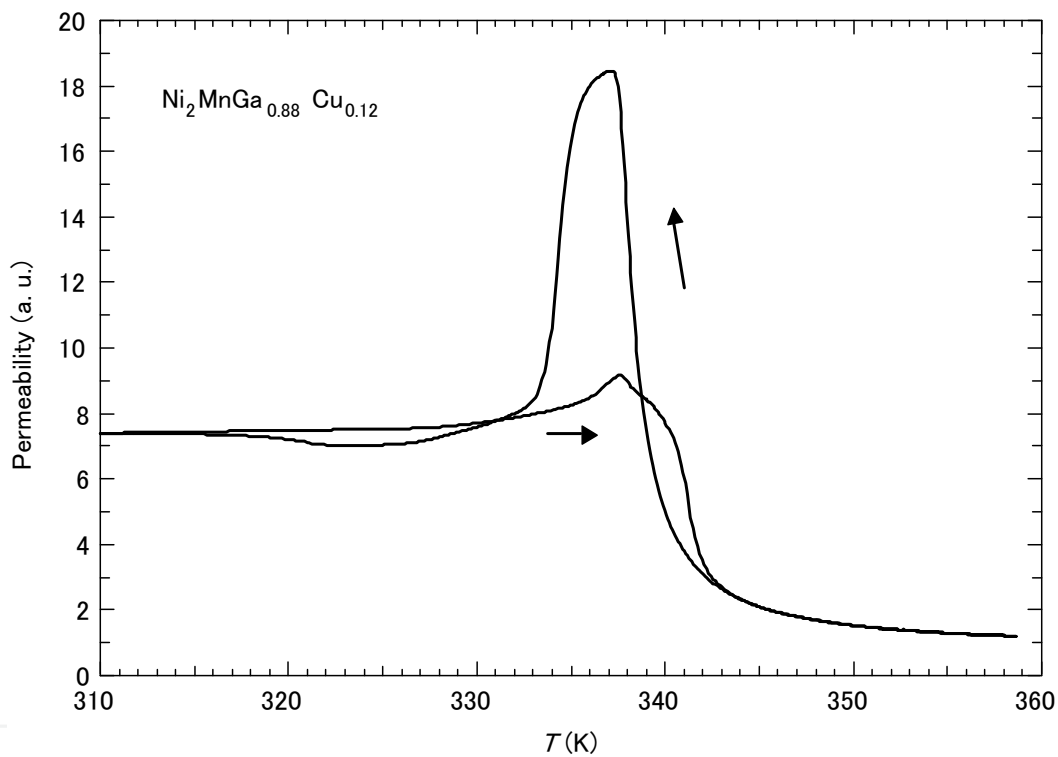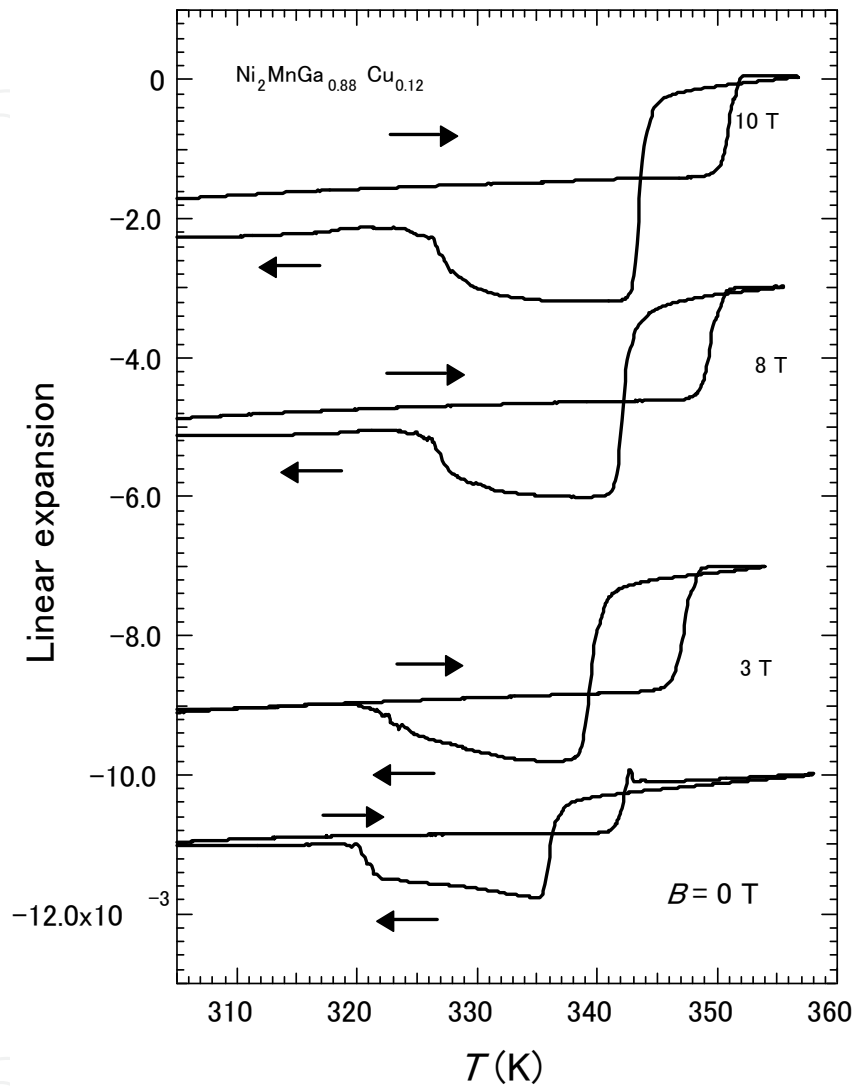

T. Sakon

Figure 8. Temperature dependence of the magnetic permeability μ of $Ni_2MnGa_{0.88}Cu_{0.12}$ in AC fields with $f = 73$ Hz and $B_{max} = 0.0050$ T. The origin of the vertical axis is the reference point when the sample is empty in the pick up coil of the magnetic permeability measurement system.

The contraction at T_M under zero fields is about 1.3×10^{-3} (0.13 %). As for $Ni_{52}Mn_{12.5}Fe_{12.5}Ga_{23}$ and $Ni_2Mn_{0.75}Cu_{0.25}Ga$, the contraction occurs at martensite temperature [27]. The strain at T_M of polycrystalline $Ni_{52}Mn_{12.5}Fe_{12.5}Ga_{23}$ was estimated as 0.14 % contraction. This value is almost the same as that of $Ni_2MnGa_{0.88}Cu_{0.12}$. After zero field measurements of the linear expansion, measurements in a magnetic field were performed from 3 T to 10 T. With increasing field, T_M and T_R are gradually increased. The shifts of T_M and T_R around zero magnetic fields were estimated as $dT_M/dB = 1.3$ K/T and $dT_R/dB = 1.5$ K/T, as shown in Figure 3. This behavior is the same as that of the $Ni_{2+x}Mn_{1-x}Ga$
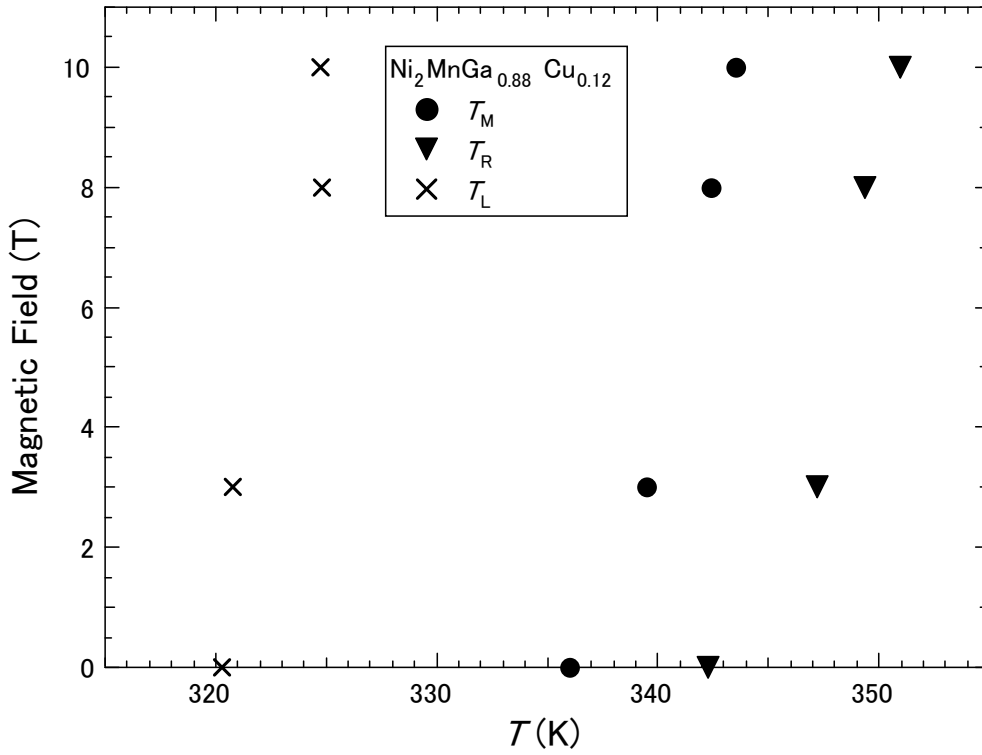
ferromagnetic alloys. The typical temperature T_L, which was defined as the kink point of the linear expansion for heating processes in Figure 9, also gradually increases with increasing fields.

T. Sakon

Figure 9. Temperature dependences of the linear thermal expansion of Ni2MnGa0.88Cu0.12, in static magnetic fields.

A noteworthy fact is that the dip of linear expansion measurements in magnetic fields is larger than that in zero fields. The variation of the strain between zero fields and non-zero field was observed for Ni2.19Mn0.81Ga [28]. The contraction in magnetic fields was larger than that in zero fields. The reason is considered that the magnetic moments of Mn and Ni atoms are aligned parallel to the magnetic field just below T_M and the *14M* and/or *D022* tetragonal lattices are rearranged by the magnetic moments. Therefore the rearrangement of these lattices due to magnetic fields occurred in high magnetic fields.
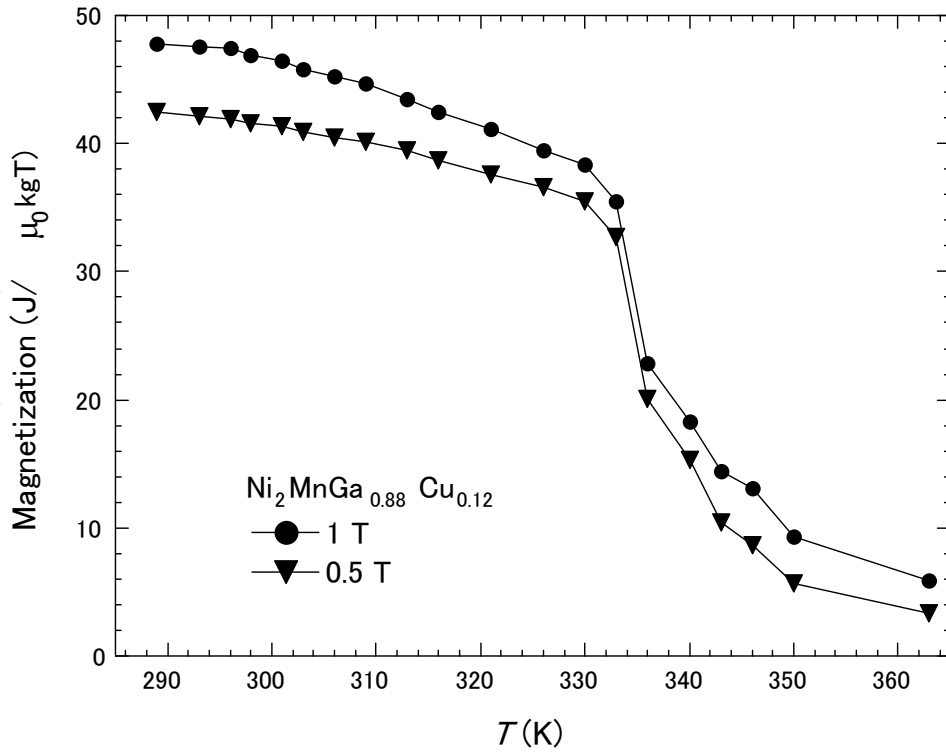
T. Sakon

Figure 10. Magnetic phase diagram of Ni₂MnGa0.88Cu0.12. Filled circles indicate the martensitic transition temperature T_M. Filled triangles indicate reverse martensitic temperature T_R. Crosses indicate the typical temperature T_L.

Figure 11 (a) shows the magnetization of Ni₂MnGa0.88Cu0.12 in a pulsed magnetic field up to 10 T. The unit of the magnetization M, J/$\mu_0$kgT in SI unit system is equal to emu/g in CGS unit system. The hysteresis of the M-B curve is considerably small. In other magnetic material, for example Gd₃Ga₅O₁₂, the magnetocaloric effect was reported [21]. They performed the magnetization measurements at initial temperature 4.2 K, then the magnetic contribution to heat capacity is comparable to the lattice heat capacity. In our experiment, the temperature change of the sample due to the magnetocaloric effect is considered within 1 K. This is due that these experiments were performed around room temperature, then the lattice heat capacity is much larger than the heating or cooling power by the magnetocaloric effect. Figure 11 (b) shows the magnetization of Ni₂MnGa0.88Cu0.12 in a pulsed magnetic field up to 2.2 T. The M-B curves with increasing field processes are shown. The M-B curves show ferromagnetic behavior below 333 K. The prominent decrease of magnetization occurred between 333 K and 336 K. Figure 12 shows the temperature dependence of the magnetization M-T at 0.5 T and 1 T, which were obtained by magnetization measurements in pulsed magnetic fields. A sudden decrease is apparent between 333 K and 336 K for each field. This temperature region corresponds to the sharp increase of the permeability when heating from low temperature in Figure 8, and just below T_M, which was obtained by the linear expansion measurement in Figure 9. The M-T curve shows a shallow depression between 310 K and 330 K, which corresponds to the dip of the permeability and the linear expansion results.
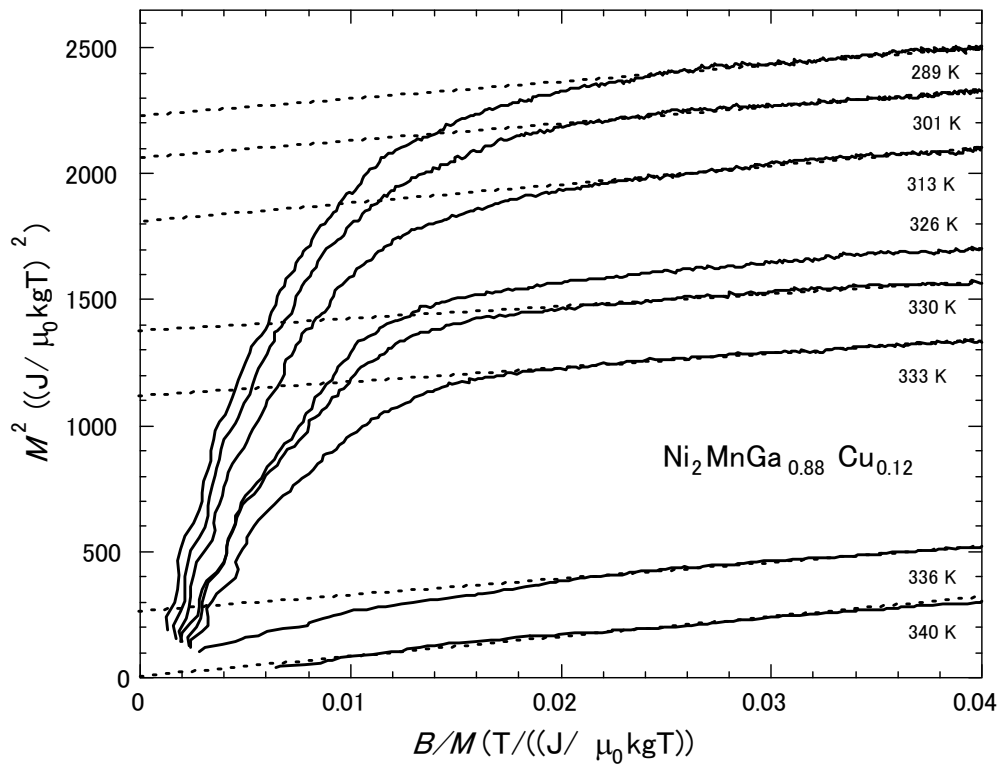
(a)

(b)
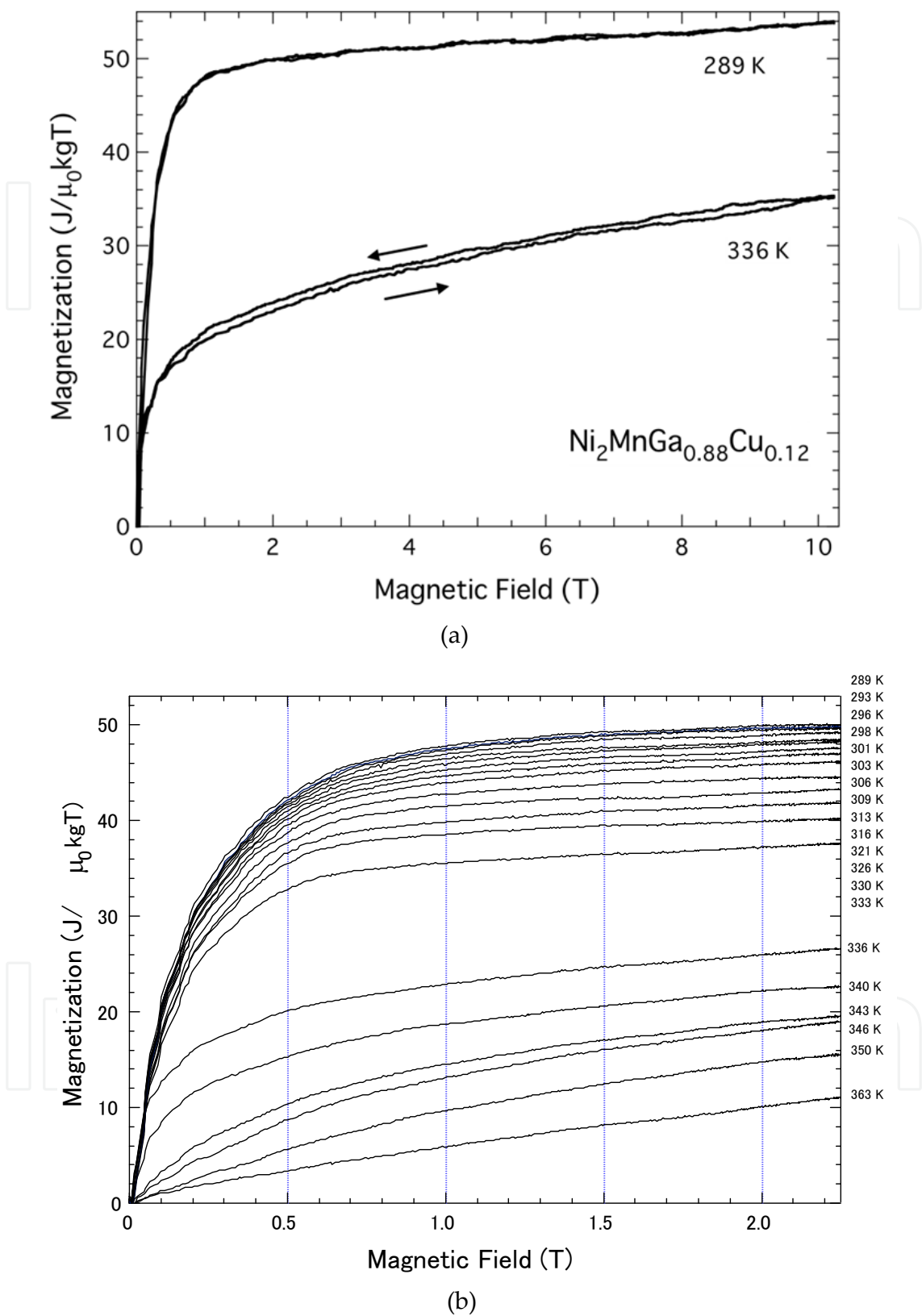
T. Sakon

Figure 11. (a). Magnetization of Ni₂MnGa₀.₈₈Cu₀.₁₂ in a pulsed magnetic field up to 10 T. (b). Magnetization of Ni₂MnGa₀.₈₈Cu₀.₁₂ in a pulsed magnetic field up to 2.2 T.

T. Sakon

Figure 12. *M-B* curves of Ni₂MnGa₀.₈₈Cu₀.₁₂.

T. Sakon

Figure 13. Arrott plot of the magnetization of Ni₂MnGa₀.₈₈Cu₀.₁₂. Dotted straight lines are extrapolated lines.

Figure 13 shows the Arrott plot of Ni₂MnGa₀.₈₈Cu₀.₁₂. The spontaneous magnetization at 289 K in a Ferro-M state is 47.1 J/$\mu_0$kgT. The obtained T_C of the martensite phase by Arrott plots in Figure 13 is 340 K, which is almost the same as T_M = 337 K. This is consistent with the x-T phase diagram of Ni₂MnGa$_{1-x}$Cu$_x$, which is obtained in reference 19.

Figure 14 shows the magnetization of Ni₂MnGa₀.₈₈Cu₀.₁₂ in a pulsed high magnetic field up to 18.6 T. The difference of the magnetization between 333 K and 336 K is clearly seen. In high magnetic fields, an almost linear increase can be seen for each M-B curve. Ni₂Mn₀.₇₅Cu₀.₂₅Ga also shows the difference of the magnetization between 302 K and 305 K, which is little lower than T_C = 307 K or T_M = 308 K [27]. It is noticeable that the Arrott plots of Ni₂MnGa₀.₈₈Cu₀.₁₂ left a space between 333 K and 336 K, and Ni₂Mn₀.₇₅Cu₀.₂₅Ga also left a space between 302 K and 303 K. The spontaneous magnetizations of Ni₂MnGa₀.₈₈Cu₀.₁₂ are 33.4 J/$\mu_0$kgT at 333 K and 16.7 J/$\mu_0$kgT at 336K, which was obtained by the Arrott plot shown in Figure 13. As for Ni₂Mn₀.₇₅Cu₀.₂₅Ga, the spontaneous magnetizations are 40.0 J/$\mu_0$kgT at 302 K and 28.3 J/$\mu_0$kgT at 303 K.
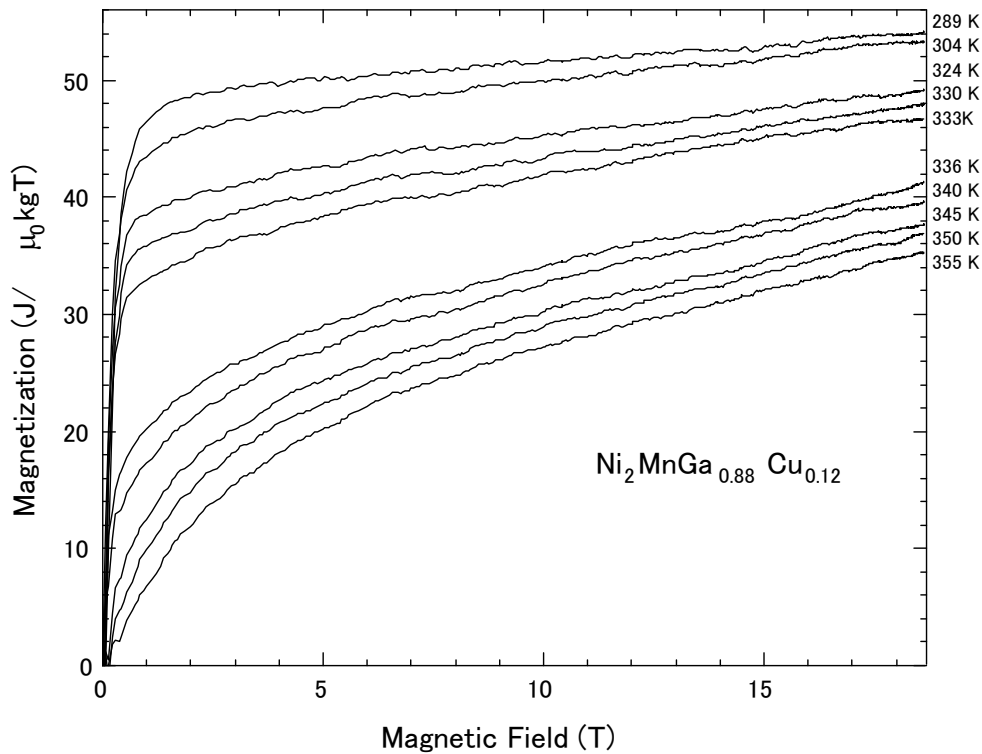
T. Sakon

Figure 14. Magnetization of Ni₂MnGa₀.₈₈Cu₀.₁₂ in a pulsed high magnetic field.

3.3. Ni₅₂Mn₂₅Ga₂₃

Figure 15 shows the temperature dependence of permeability. When heating from 300 K, permeability increases gradually. As shown in Figure 15, permeability increases above 330 K and suddenly decreases around 360 K. When cooling from a high temperature, permeability shows a sudden increase at about 356 K and decreases at 325 K. The sudden changes in

permeability indicate that the ferrromagnetic transition occurs around 358 K. The temperature dependence of permeability for $Ni_{52}Mn_{25}Ga_{23}$ is similar to that for $Ni_{52}Mn_{12.5}Fe_{12.5}Ga_{23}$, which shows a transition of a ferromagnetic–martensite (Ferro–M) phase to a ferromagnetic–austenite (Ferro–A) phase [29]. The step around 330 K (heating process) and 325 K (cooling process) reflects stronger magnetic anisotropy in the tetragonal martensite phase [8,18]. Polycrystalline $Ni_{49.5}Mn_{28.5}Ga_{22}$, $Ni_{50}Mn_{28}Ga_{22}$ and $Ni_{52}Mn_{12.5}Fe_{12.5}Ga_{23}$ alloys also indicate the magnetization (or permeability) step at T_M [9,18,27] below the field of 10 mT.
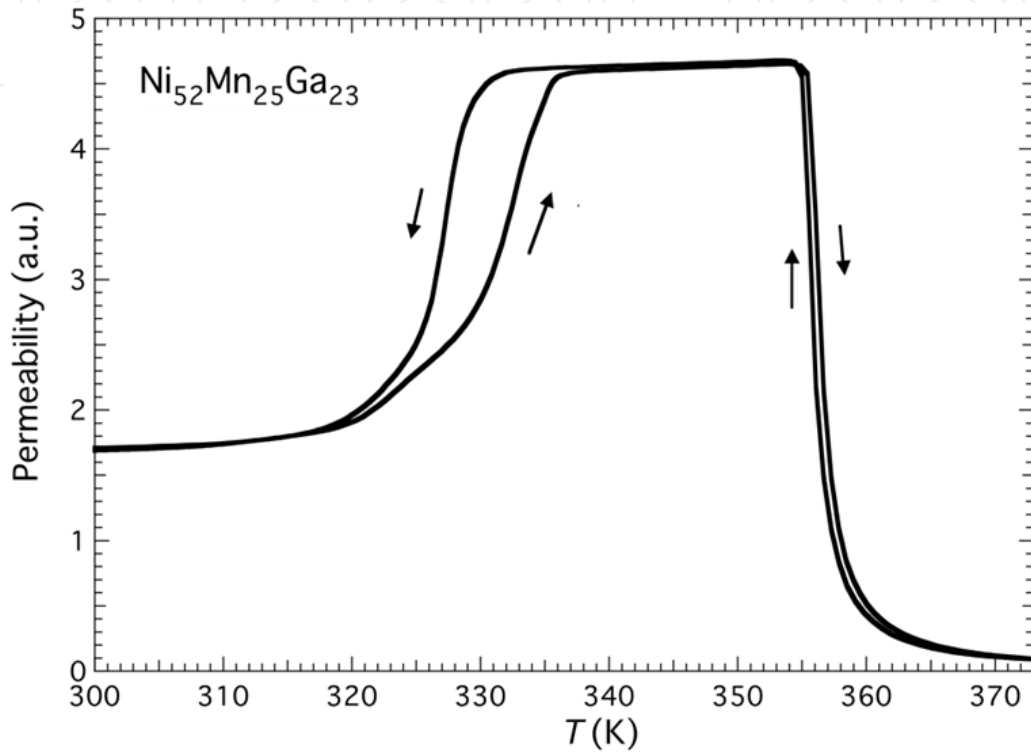
T. Sakon

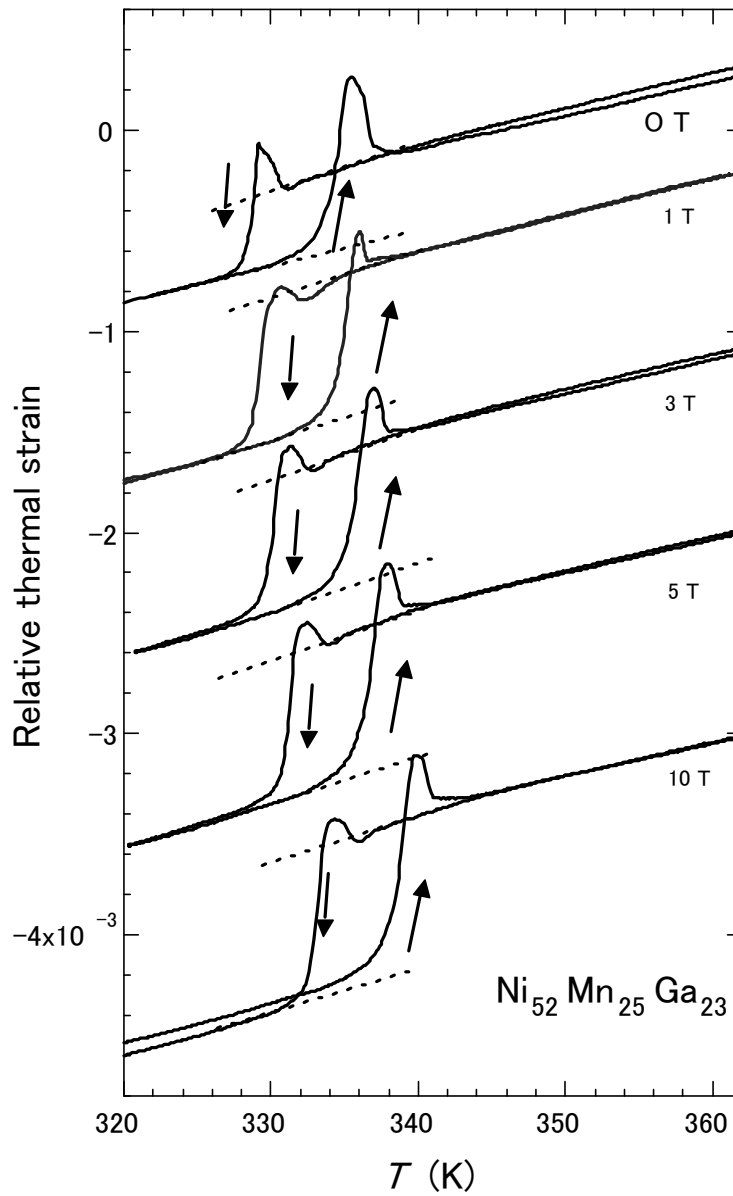**Figure 15.** Temperature dependence of the magnetic permeability μ of $Ni_{52}Mn_{25}Ga_{23}$ in AC fields with f = 73 Hz and B_{max} = 0.0050 T. The origin of the vertical axis is the reference point when the sample is empty in the pickup coil of the magnetic permeability measurement system.
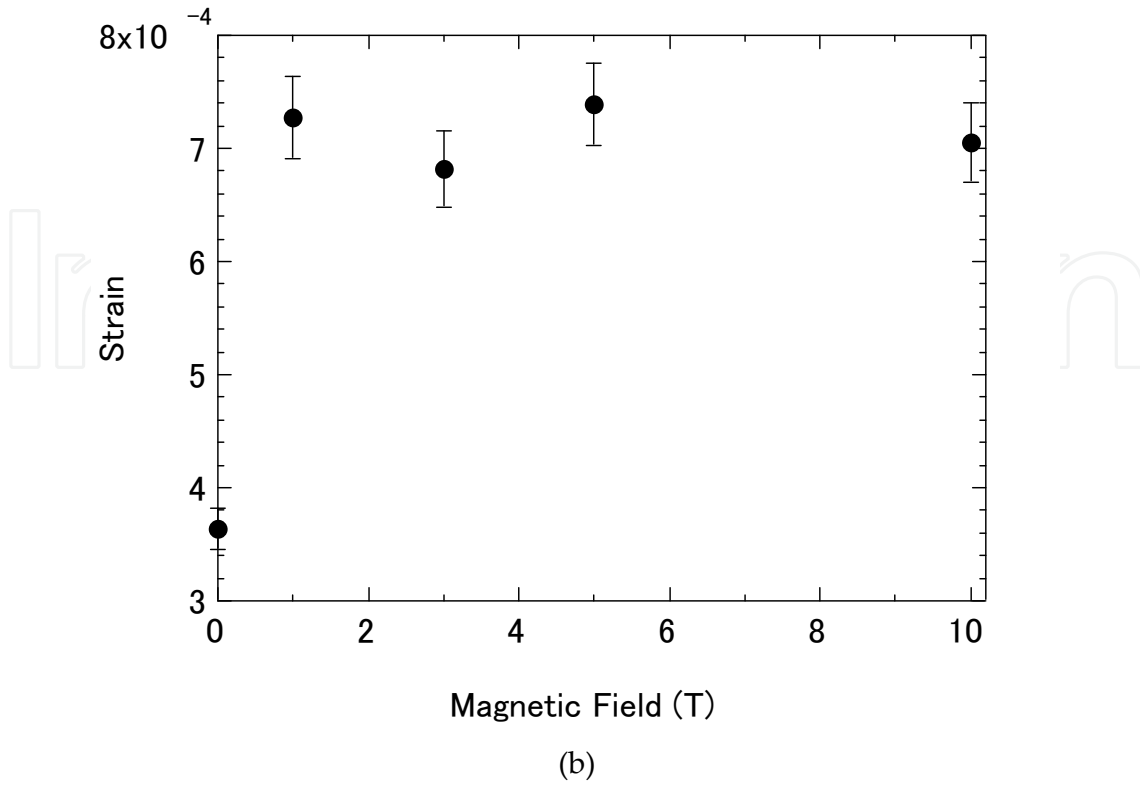
Figure 16 (a) shows the linear thermal strain of $Ni_{52}Mn_{25}Ga_{23}$. Solid lines are the experimental data and dotted lines are the extrapolated lines. At zero magnetic fields, the memory strain was observed, as polycrystalline $Ni_{53.6}Mn_{27.1}Ga_{19.3}$ [10]. When heating from 300 K, slight strain is observed first at zero magnetic fields. Around 334 K, a sharp strain is observed. The results of previous studies [6,7] suggest that this is because of the reverse martensite transition T_R = 334 K, which is defined as the midpoint temperature of the transition. When cooling from 370 K, a sudden decrease is observed at 328 K. Given the lattice structure, the martensite transition temperature T_M is 328 K. The permeability at the Ferro–M phase is very low compared with that at the Ferro–A phase. The results of permeability and linear strain measurements indicate that the region above T_M is a Ferro–A phase and that below T_M is a Ferro–M phase. The permeability measurement results indicate that the ferromagnetic transition from the paramagnetic–austenite (Para–A) phase to the

Ferro–A phase occurs around 358 K (see Figure 15). On the other hand, the linear strain does not show noticeable anomaly at the ferromagnetic transition around 358 K.

When cooling from 370 K, the thermal strain shows a peak at 329 K. This may be attributed to the intermingling of the $L2_1$ austenite lattices and the $M14$ martensite lattices at the martensite transition. The sequential phenomenon is observed in single crystalline $Ni_{2.19}Mn_{0.81}Ga$ [31]. Zhu *et al.* suggests that the small satellite peaks in heat flow plot, which flanks the central peak indicates the structural transition takes place in multiple steps [11]. The contraction at T_M under zero fields is about 0.5×10^{-3} (0.05%). As for other Heusler alloys, $Ni_{52}Mn_{12.5}Fe_{12.5}Ga_{23}$ and $Ni_2Mn_{0.75}Cu_{0.25}Ga$, the contraction occurs at martensite temperature [27]. The strain at T_M of polycrystalline $Ni_{52}Mn_{12.5}Fe_{12.5}Ga_{23}$ was estimated as 0.14% contraction. This value is larger than that of $Ni_{52}Mn_{25}Ga_{23}$. After zero field measurements of the linear strain, measurements in

(a)

T. Sakon

Figure 16. (a). Temperature dependence of the linear thermal strain of $Ni_{52}Mn_{25}Ga_{23}$ in static magnetic fields. The dotted lines are the extrapolated lines of the thermal strain. (b). Magnetic field dependence of the strain at the martensite transition temperature obtained from the thermal strain in Figure. 16 (a).

magnetic fields from 1 T to 10 T were performed. The strain at T_M under the magnetic field of 1 T was estimated as 0.10% contraction, which is twice that under zero magnetic field (0.05%). These results indicate that the magnetic fields influence the structural phase transition. After these thermal cycles in magnetic fields, the thermal strain in zero fields was 0.05 % contraction, which is as same as the first cycle in zero fields. Around 358 K, which is the ferromagnetic transition temperature, no anomaly was observed in the magnetic fields. Figure 16 (b) shows the magnetic field dependence of the strain at T_M. At zero field, the strain is 3.6×10^{-4}. On the other hand, the strain in a magnetic field is about 7.1×10^{-4}, which is almost twice that in zero field. Ullakko *et al*. measured the magnetic-field-induced strain of a Ni₂MnGa single crystal [1]. The strain at T_M in zero field was 2×10^{-4}. This is only a small fraction compared with the lattice constant change for *c*-axis from the austenite to martensite phases, which was $\Delta c / c = 6.56\%$. It is proposed that the strain accommodation is occurred by different twin variant orientations. As shown in Figure. 16 (b), the thermal strain under the magnetic field of 1 T was 7.2×10^{-4}, indicating the field aligned some of the twin variants.

In the martensite phase, the magnetic moment in the magnetic easy direction was coupled with the strain along the short *c*-axis of the martensite variant structure. As a result, under the applied magnetic field, the variant rearrangement occurs with the assistance of twin boundary motion, such that the magnetic easy axis is parallel to the applied field. Therefore,

the total magnetic free energy is minimal. The variant rearrangement results in field influence on the thermal expansion as shown in Figure 16(b).

Variation in the strain between zero field and non-zero field was observed for $Ni_{2.19}Mn_{0.81}Ga$ and $Ni_{2.20}Mn_{0.80}Ga$ polycrystalline samples [30]. The change in the sample length by means of the thermal strain measurements at the martensite phase transition was 0.04 % for $Ni_{2.19}Mn_{0.81}Ga$ and 0.12 % for $Ni_{2.20}Mn_{0.80}Ga$. The thermal strain for $Ni_{2.19}Mn_{0.81}Ga$ in the presence of 1.4 T magnetic field, the change was increased to 0.13 %, which means 3.2 times increase of the strain. The increase of the strain was 2.6 times (0.31 % strain) for $Ni_{2.20}Mn_{0.80}Ga$. The variation in the strain between zero fields and non-zero field was also observed for $Ni_{49.6}Mn_{27.3}Ga_{23.1}$ polycrystalline samples [31]. With increasing measuring magnetic fields, the difference in the strain increased. Aksoy *et al.* proposed that the strain increase is due to increase of the preferred alignment of the short *c* axis along the applied field, and, high twin boundary mobility in Ni-Mn-Ga is expected to be the main case of the alignment, although the martensite variant nucleation with preferred *c* axis orientation in the external field already just at the martensite transition temperature is also the influence of the shrinkage [31]. Further they mentioned that, when a sample was cooled from the austenite down to the martensite phase in zero fields, no preferred orientation is given to the variant growth during nucleation, whether the easy axis is a long axis or a short axis. When a magnetic field is applied in the austenite phase and the sample is cooled down through T_M in the constant field, a preferred growth direction is provided to the variants. Consequently, the variants with easy axis along the applied field direction nucleate more and more. If the easy axis is short axis, the sample length decreases. Then the contraction at T_M is observed in thermal strain measurements.

As for Ni_2MnGa single crystal, in zero-field cooling process, strains of nearly 0.02 % have been observed at T_M = 276 K [1]. The strain at transformation in 1.0 T is 0.145 %, indicating that the field has aligned some of the twin variants. Now we compare the strain and the magnetization results of $Ni_{2+x}Mn_{1-x}Ga$ alloys [28]. For the alloys which showed increase of the strain for *x* = 0.18 and 0.20, the T_M and T_c are almost same temperature. Consequently, the magnetization change is large. For these composition alloys, clear hysteresis in the magnetization was observed, which indicates first order magnetic transition. From these results, it is supposed that the magnetic field influences the orientation of the easy *c* axis along the magnetic field. As for $Ni_{52}Mn_{25}Ga_{23}$, The magnetization change is large at T_M, as shown in Figure 22. The permeability in Figure 15 shows clear change and hysteresis, which indicates the first order transition. It is also supposed that the magnetic field influences the orientation of the easy *c* axis along the magnetic field, and then the variant rearrangement was occurred. Consequently, the variation in the strain between zero fields and non-zero field was observed.

Figure 17 shows the magnetic-field-induced strain at 300 K (Ferro–M phase) in a static magnetic field. When increasing the magnetic field from zero fields, a sudden contraction occurs up to 1 T. Above 1 T, a gradual contraction is observed. When decreasing the magnetic field from 10 T, a modicum of strain occurs. Below 1 T, a sudden strain is observed. The magnetic-field-induced strain at 10 T is −100 ppm or −0.010%, which is considerably smaller than the contraction value at T_M. The sudden contraction between 0 and 1 T when increasing

the field is supposed to be related to the temperature dependences of the linear strains between zero fields and above 1 T and below T_M. The variant rearrangement results in a magnetic-field-induced strain, which is the origin of the magnetostriction shown in Figure 17. The reason of smallness of the magnetic field induced strain is supposed that; when the sample is cooled down from the austenite phase to the martensite phase in a constant field, variant arrangement is occurred and the contraction is occurred, as mentioned above. In zero fields, cooling from the austenite phase to the martensite phase, the variant arrangement is fixed. When the magnetic field is applied with constant temperature, the variant rearrangement is considered to be difficult. Therefore the magnetic field induced strain is smaller than the strain at T_M. in the linear strain measurements.
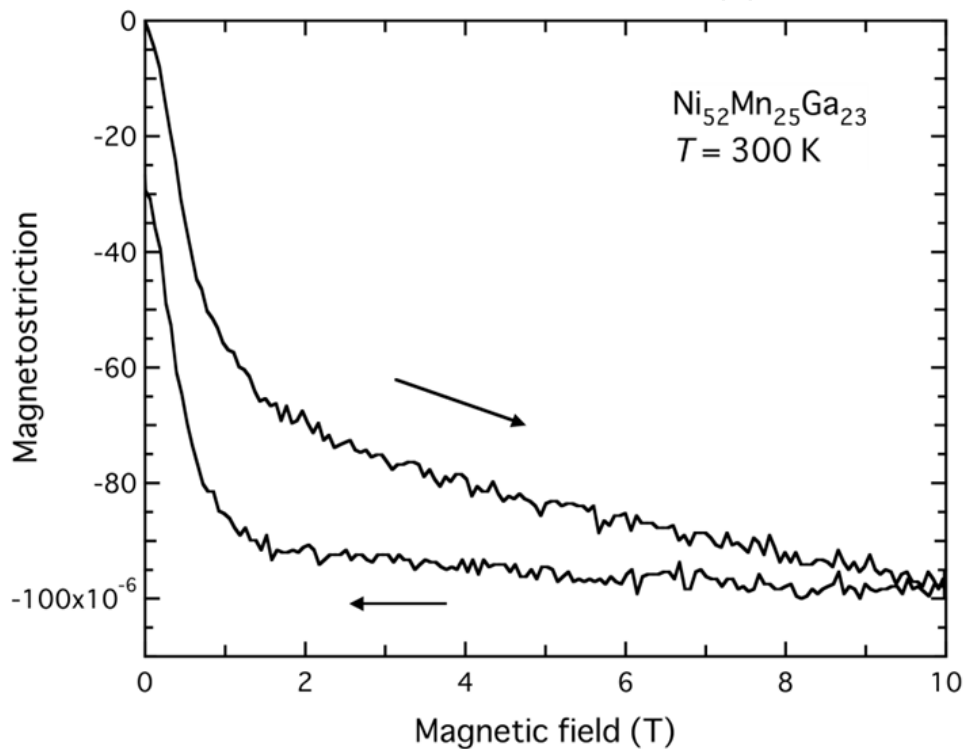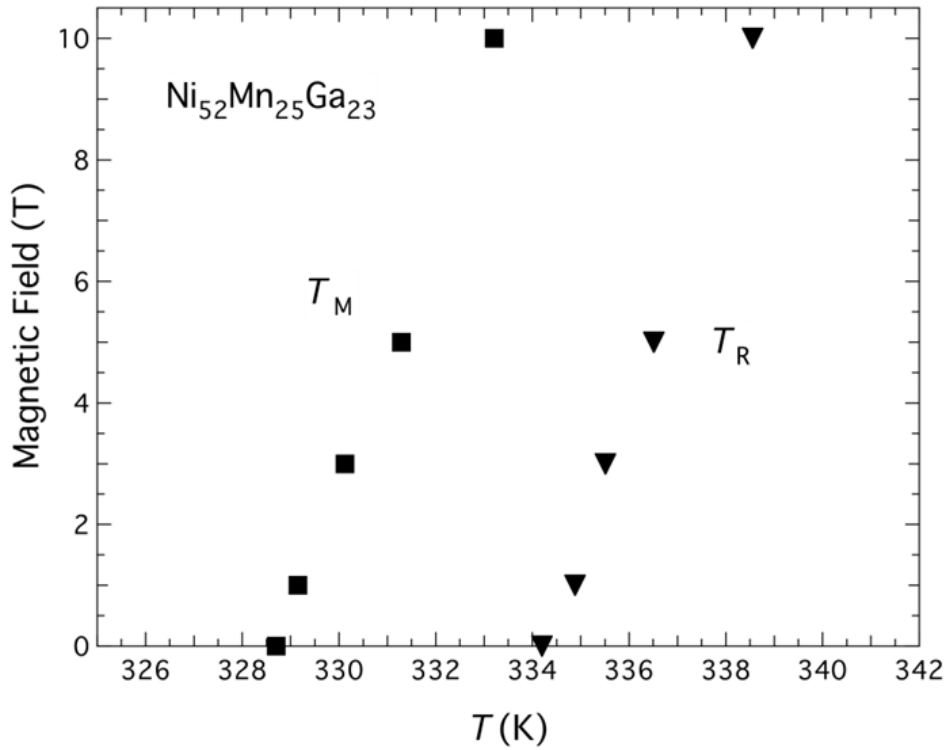

T. Sakon

Figure 17. Magnetostriction of Ni₅₂Mn₂₅Ga₂₃ at 300 K in a static magnetic field up to 10 T.

The magnetic-field-induced strain of the polycrystalline Ni₅₀Mn₂₈Ga₂₂ alloy was reported by Murray *et al.* [18]. They mentioned that the strain in the martensite phase below T_M is an order of magnitude smaller than that of a single crystal of the stoichiometric compounds [1]. They attributed this to the polycrystalline nature of the material or to the presence of impurities that impede twin boundary motion. The field-induced strain of Ni₅₀Mn₂₈Ga₂₂ increases on cooling from the austenite phase, leading to an abrupt increase with the appearance of the twin variant below T_M. On heating from the martensite phase, an abrupt increase occurs in the field-induced strain around T_M. They suggest that this is caused by lattice softening near T_M. As for the thermal strain of Ni₅₂Mn₂₅Ga₂₃, shown in Figure 16 (a), peaks appear for both T_M and T_R in zero field and all values of the magnetic field. The peak at T_R, associated with heating, is larger than that at T_M, associated with cooling. These peaks

indicate that the lattice expands abruptly. Dai *et al.* studied the elastic constants of a $Ni_{0.50}Mn_{0.284}Ga_{0.216}$ single crystal using the ultrasonic continuous-wave method [31]. C_{11}, C_{33}, C_{66}, and C_{44} modes were investigated; every mode indicated abrupt softening around T_M. This lattice softening appears to be affected by the abrupt expansion just above T_M when cooling from the austenite phase.

Figure 18 shows the magnetic phase diagram of $Ni_{52}Mn_{25}Ga_{23}$. With increasing field, T_M and T_R gradually increase. The shifts in T_M and T_R around zero magnetic field are estimated as $dT_M/dB = 0.46$ K/T and $dT_R/dB = 0.43$ K/T, which are similar to those of the $Ni_{52}Mn_{12.5}Fe_{12.5}Ga_{23}$ alloy ($dT_M/dB = 0.5$ K/T) [27].

T. Sakon

Figure 18. Magnetic phase diagram of $Ni_{52}Mn_{25}Ga_{23}$. Filled squares indicate the martensite transition temperature T_M. Filled triangles indicate reverse martensite temperature T_R.

Figure 19 shows the magnetization curves of $Ni_{52}Mn_{25}Ga_{23}$ in a pulsed magnetic field up to 2.2 T. The unit of magnetization M is J/μ_0kgT in the SI unit system or emu/g in the CGS unit system (both having identical numerical values). The M–B curves were measured from low temperature. The hysteresis of the M–B curve is considerably small. The magneto caloric effects in other magnetic materials were also reported; for example, Levitin *et al.* reported for $Gd_3Ga_5O_{12}$ [32]. They performed magnetization measurements at an initial temperature of 4.2 K, where the magnetic contribution to heat capacity is comparable to the lattice heat capacity. In our experiment, the temperature change of the sample due to the magneto caloric effect is considered to be within 1 K. This is because these experiments were performed around room temperature, where the lattice heat capacity is much larger than the heating or cooling power by the magneto caloric effect.
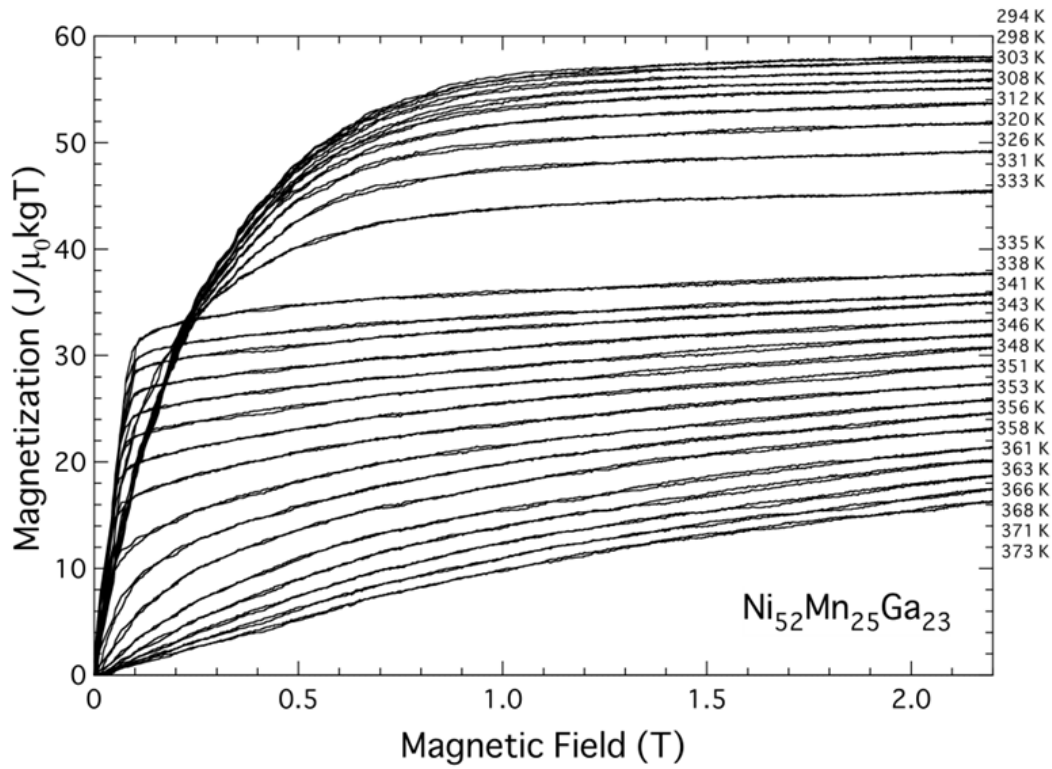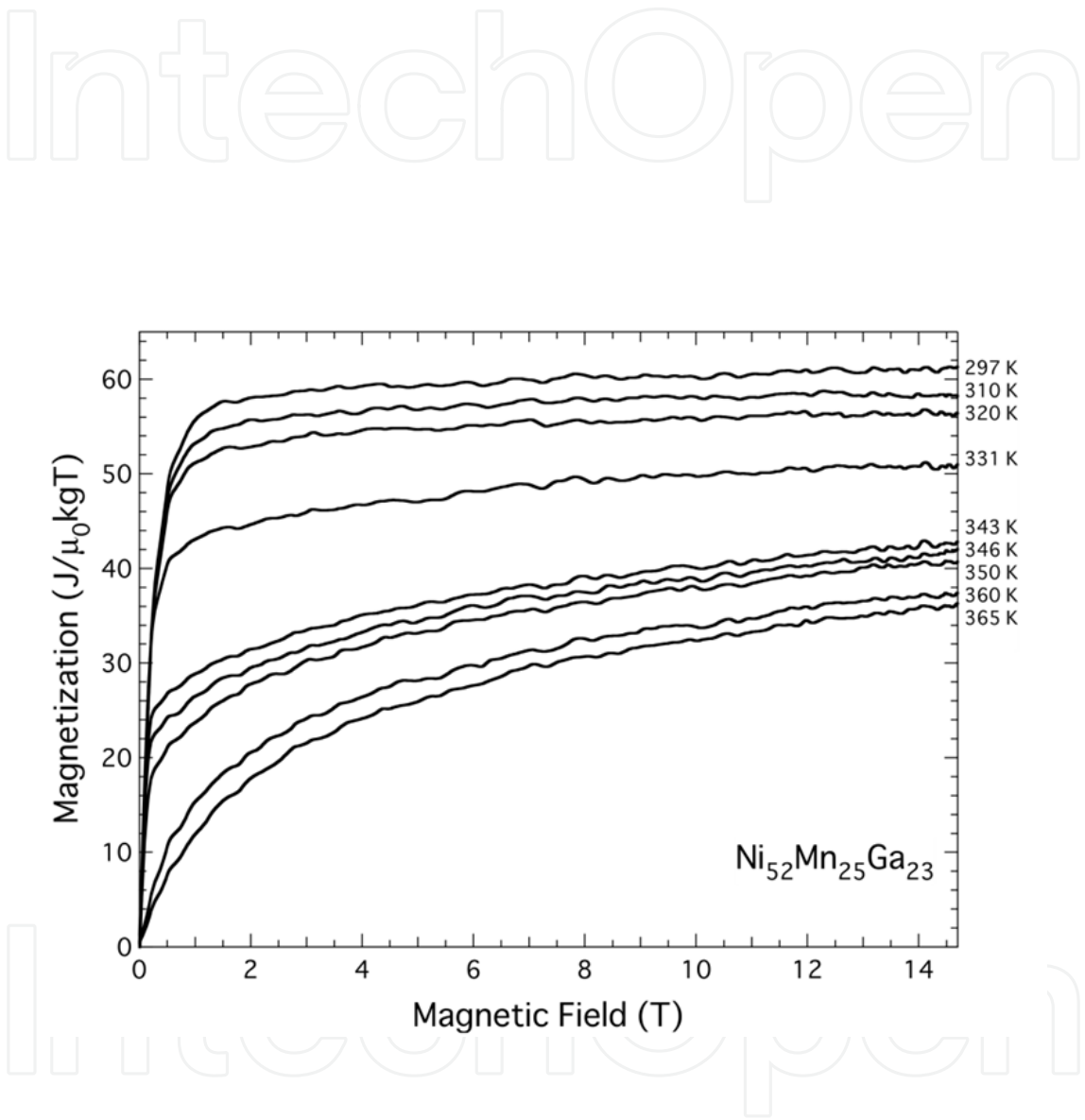
T. Sakon

Figure 19. Magnetization of Ni$_{52}$Mn$_{25}$Ga$_{23}$ in a pulsed magnetic field up to 2.2 T.

The *M–B* curves show ferromagnetic behavior below 356 K. It is clear that the field dependence of the magnetization at the Ferro–A phase above T_R = 334 K is different from that at the Ferro–M phase below T_R. At the Ferro–M phase, magnetization increases with magnetic fields. On the other hand, at the Ferro–A phase between 334 and 356 K, a sudden increase in magnetization occurs between 0 and 0.1 T.

Figure 20 shows magnetization in a magnetic field up to 15 T. In high magnetic fields, an almost linear increase can be seen for each *M–B* curve. In particular, as for the *M–B* curve below 334 K, the high magnetic field susceptibility is quite small.

Figure 21 shows the Arrott plot of Ni$_{52}$Mn$_{25}$Ga$_{23}$. The spontaneous magnetization at 294 K in a Ferro–M phase is 55.0 J/$\mu_0$kgT. The Curie temperature of the austenite phase T_{CA} determined by Arrott plots in Figure 21 is 358 K. This is consistent with the *x–T* phase diagram of Ni$_{50+x}$Mn$_{25}$Ga$_{25-x}$ [6,7]. In high magnetic fields, an almost linear increase can be seen for each *M–B* curve. Ni$_2$Mn$_{0.75}$Cu$_{0.25}$Ga also shows the difference in magnetization between 302 and 305 K, which is somewhat lower than T_C = 307 K or T_M = 308 K [27]. Note that the Arrott plots of Ni$_{52}$Mn$_{25}$Ga$_{23}$ left a space between 333 and 335 K, and Ni$_2$Mn$_{0.75}$Cu$_{0.25}$Ga left a space between 302 and 303 K. The spontaneous magnetizations of Ni$_{52}$Mn$_{25}$Ga$_{23}$ are 42.2 J/$\mu_0$kgT at 333 K and 34.2 J/$\mu_0$kgT at 335 K, which were obtained by the Arrott plot shown in Figure 21. As for Ni$_2$Mn$_{0.75}$Cu$_{0.25}$Ga, the spontaneous magnetizations are 40.0 J/$\mu_0$kgT at 302 K and 28.3 J/$\mu_0$kgT at 303 K.

T. Sakon

Figure 20. Magnetization of Ni₅₂Mn₂₅Ga₂₃ in a pulsed magnetic field up to 15 T.
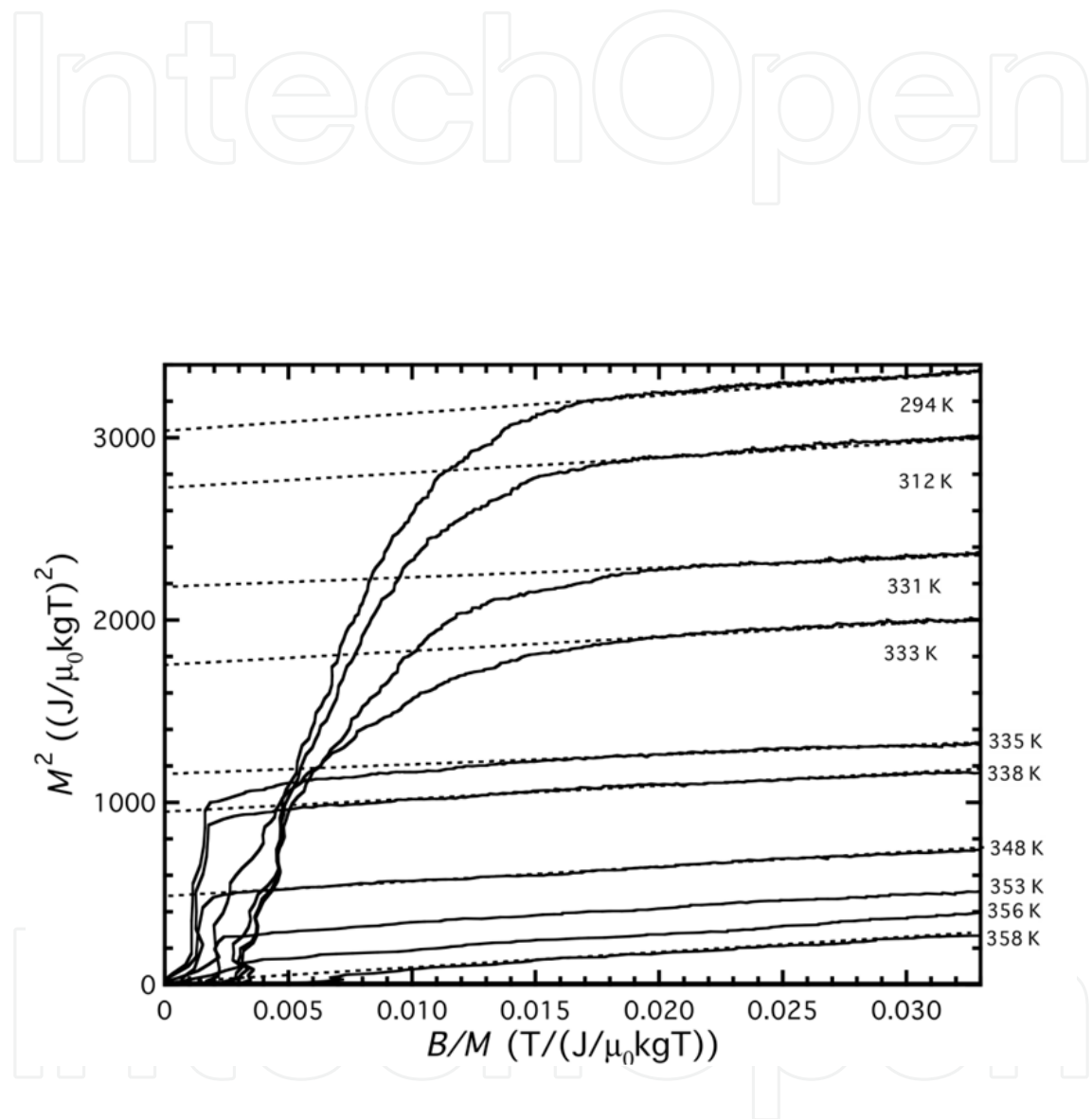
Figure 21. Arrott plot of the magnetization of Ni₅₂Mn₂₅Ga₂₃. Dotted straight lines are extrapolated lines.

T. Sakon

Figure 22 shows the temperature dependence of the magnetization M–T at 0.1, 0.5, and 1 T, which was obtained by magnetization measurements in pulsed magnetic fields. Open circles are the spontaneous magnetizations, which was obtained by the Arrott plot method. A sudden decrease is apparent between 333 and 336 K for each field, and also the spontaneous magnetization. This temperature region corresponds to the sharp increase in permeability when heating from low temperature in Figure 15, and just below T_R, which was obtained by the linear strain measurement in Figure 16 (a).

The M-T curve in Figure 22 can be seen as the combination of two single-phase M-T curves. One corresponds to the martensite phase, and the other corresponds to the austenite phase. The obtained Curie temperatures in the martensite phase and the austenite phase are T_{CM} = 333.5 ± 0.5 K and T_{CA} = 358.0 ± 0.5 K. This is due to the difference of the ferromagnetic interactions for both structural phases. These analyses of magnetic properties in $Ni_{51.9}Mn_{23.2}Ga_{24.9}$ were also reported in reference 11.

It is well known that the tetragonal martensite Ni–Mn–Ga has higher magnetocrystalline anisotropy in association with the multi-dominant structure of the martensite phase. Consequently, lower initial permeability and higher coercivity than the cubic austenite Ni–Mn–Ga alloys can occur [8,11–13,15]. The martensite transition occurs in the ferromagnetic phase, and the decrease in magnetization is observed at intermediate fields for $0 < B < 0.5$ T, as shown in Figure 22. This property is also shown by magnetization in many Ni–Mn–Ga alloys (e.g., $Ni_{49.5}Mn_{25.4}Ga_{25.1}$) and Ni–Mn–Sn alloys (e.g., $Ni_{50}Mn_{35}Sn_{15}$) [8,33,34]. Consequently, at low field, the austenitic Ni–Mn–Ga (with softer ferromagnetism) shows an abrupt increase in M, while the martensite Ni–Mn–Ga (with harder ferromagnetism) shows gradual increase in M with the field. On the other hand, the martensite Ni–Mn–Ga (in low-temperature phase) has higher saturation magnetization (typically, M_s increases with decreasing temperature) than the austenite Ni–Mn–Ga. As a result, at very high field or saturation field (>1 T), magnetization of the martensite is higher than that of the austenite, as shown in Figures 20 and 22. As for other Ni–Mn–Ga alloys, Kim et al. reported magnetization in a $Ni_{2.14}Mn_{0.84}Ga_{1.02}$ single crystal, which shows a transition from the Ferro–A phase to Ferro–M phases with $14M$ structure [14]. The magnetization curve in $Ni_{2.14}Mn_{0.84}Ga_{1.02}$ at 290 K, just below the martensite transition temperature, sharply bend at the critical field, B_s = 0.6 T, and above 0.6 T, the magnetization slightly increases with increasing fields. On the other hand, a bend in the magnetization is not clear. We defined the critical field B_s in $Ni_{52}Mn_{25}Ga_{23}$ as the field where the magnetization Arrott plot was off from the extrapolated linear line, which is illustrated by the dotted line in Figure 21, and obtained B_s as 0.84 T, which is of the same order as that in $Ni_{2.14}Mn_{0.84}Ga_{1.02}$. The magnetization is the same as that in $Ni_{52}Mn_{25}Ga_{23}$. The magnetic anisotropy constant K_U in a Ni_2MnGa single crystal is 1.17×10^5 J/m^3 (11.7×10^5 erg/cm^3) in the martensite phase and 2.7×10^4 J/m^3 (2.7×10^5 erg/cm^3) in the austenite phase [1], indicating that the magnetic anisotropy is about four times larger in the martensite phase than that in the austenite phase. The Zeeman energy and/or magnetocrystalline anisotropy energy that is sufficient to induce motion of the twin boundary is denoted as $M_sB_s/2 = K_U$ [1]. Kim et al. also mentioned that the magnetocrystalline anisotropy energy is of the order of 10^5 J/m^3 [14]. The spontaneous magnetization in $Ni_{52}Mn_{25}Ga_{23}$ at 333 K, just below T_R is 42.2

J/$\mu_0$kgT, which was obtained by the Arrott plot in Figure 22. When using this value as M_S, the magnetocrystalline anisotropy energy in the martensite phase of $Ni_{52}Mn_{25}Ga_{23}$ is $M_S B_S/2 = K_U$ $= 1.04 \times 10^5$ J/m³, which is on the same order as that in the martensite phase of Ni₂MnGa. These magnetic properties were also shown for $Ni_{51.9}Mn_{23.2}Ga_{24.9}$ [11], $Ni_{49.5}Mn_{25.4}Ga_{25.1}$ [12], and $Ni_{54}Mn_{21}Ga_{25}$ [13].
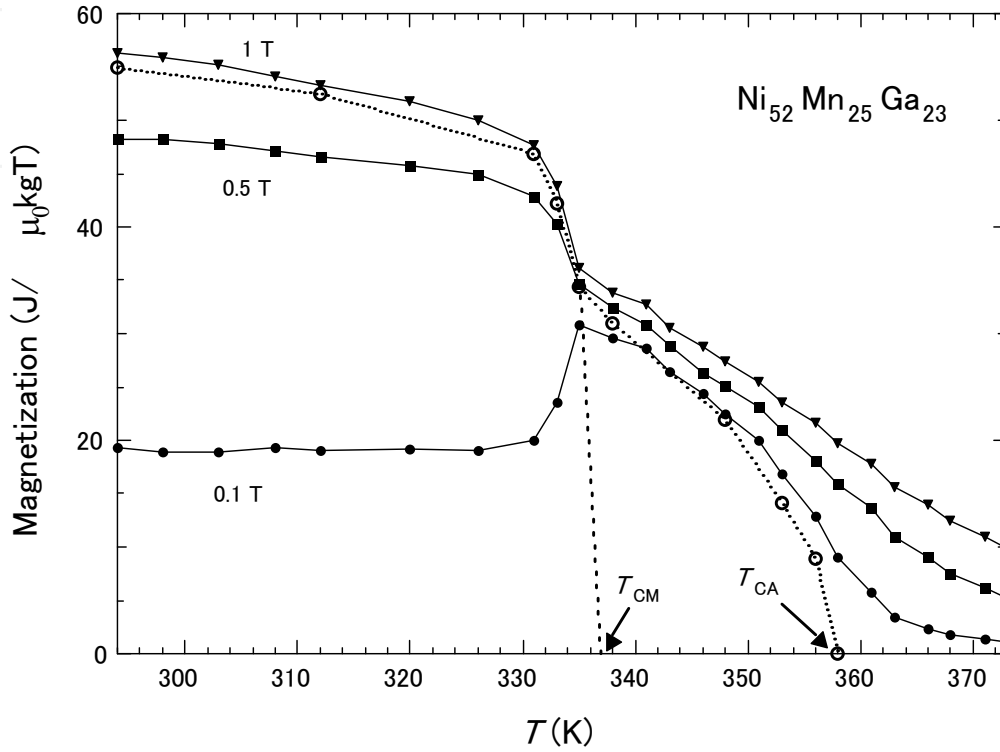
T. Sakon

Figure 22. Temperature dependence of the magnetization of Ni₅₂Mn₂₅Ga₂₃. Open circles are the spontaneous magnetizations, which was obtained by the Arrott plot method. Dotted lines are extrapolated lines of the spontaneous magnetization plots. T_{CM} and T_{CA} indicate the martensite Curie temperature and the austenite Curie temperature, respectively.

The relationship between magnetism and T_M in magnetic fields is discussed for Ni₂MnGa-type Heusler alloys. Table 1 shows the spontaneous magnetizations and dT_M/dB values of $Ni_{2+x}Mn_{1-x}Ga$, $Ni_{52}Mn_{12.5}Fe_{12.5}Ga_{23}$, $Ni_2Mn_{0.75}Cu_{0.25}Ga$, $Ni_2MnGa_{0.88}Cu_{0.12}$, and $Ni_{52}Mn_{25}Ga_{23}$. As for $Ni_{2+x}Mn_{1-x}Ga$ alloys, shifts in T_M in magnetic fields were observed by magnetization measurements [2,26–28]. T_M and T_C of Ni₂MnGa ($x = 0$) are 200 and 360 K, respectively. The region above T_M is the Ferro–A phase. The sample with $x = 0$ of $Ni_{2+x}Mn_{1-x}Ga$ shows phase transition from the Ferro–A to Ferro–M phases at T_M. The sample with $x = 0.19$ shows ferromagnetic transition and martensite transition at T_M. For $x = 0$, the shift in T_M is estimated as dT_M/dB = 0.2 K/T [35] and for $x = 0.19$, dT_M/dB = 1 .0 K/T [36]. The shift in T_M for $x = 0.19$ is higher than that for $x = 0$. These results indicate that the shift in T_M for the alloy that shows Para–A to Ferro–M phase transition is larger than that for the alloy that shows Ferro–A to Ferro–M phase transition. The values of dT_M/dB are roughly proportional to the change in spontaneous magnetization, $(M_M − M_A)/M_M$, as shown in Table 1. This indicates

that the magnetic moments influence the martensite transition; in other words, the structural transition and the T_M increase in accordance with the magnetic fields are proportional to the difference between the magnetization of the austenite phase and that of the martensite phase. Therefore, it is considered that the alloys, in which T_M and T_C are close to each other, show a larger shift in T_M in magnetic fields.

Khovailo *et al.* discussed the correlation between the shifts in T_M for $Ni_{2+x}Mn_{1-x}Ga$ ($0 \leq x \leq 0.19$) using theoretical calculations [37,38]. The experimental values of this shift for $Ni_{2+x}Mn_{1-x}Ga$ ($0 \leq x \leq 0.19$) are in good agreement with the theoretical calculation results. In general, in a magnetic field, the Gibbs free energy is lowered by the Zeeman energy $-\Delta MB$ that enhances the motive force of the martensite phase transition. Thus, T_M of the ferromagnetic Heusler alloys $Ni_{52}Mn_{12.5}Fe_{12.5}Ga_{23}$, $Ni_2Mn_{0.75}Cu_{0.25}Ga$, and $Ni_2MnGa_{0.88}Cu_{0.12}$ in recent studies [27,39,40] and $Ni_{52}Mn_{25}Ga_{23}$ in this study are considered to have shifted in accordance with the magnetic fields because high magnetic fields are favorable for ferromagnetic martensite phases.

Chernenko *et al.* studied the temperature dependence of both the saturation magnetic field values and the x-ray powder diffraction patterns of Ni-Mn-Ga alloys and analyzed with the theoretical consideration [12]. The theory proposes that the free energy for ferromagnetic martensite phase, exposed to an external magnetic field, is expressed as three terms. First term is the magnetic anisotropy energy. The second and third terms describe the magnetostatic and the Zeeman energy, respectively. The c/a ratio was expressed as

$$c/a = 1 - \frac{\left[\left(H_S / M\right) + \left|D_1 - D_2\right|\right]}{12\delta},$$ (2)

where H_s indicates the saturation magnetic field. M denotes the absolute value of the magnetization. D_1 and D_2 denote the diagonal matrix elements, and δ is the dimensionless magnetoelastic parameter. The linear dependence of the magnetic anisotropy constant on the tetragonal distortion of the cubic crystal lattice arising in the course of the martensite transition.

In order to apply this theory to our present work, it is considered that further theoretical consideration is needed for apply this theory for analyzing the influence between the martensite variant structure and the magnetic field, which is reflected by the Zeeman term.

4. Conclusions

$Ni_{52}Mn_{12.5}Fe_{12.5}Ga_{23}$ and $Ni_2Mn_{0.75}Cu_{0.25}Ga$

Thermal expansion, magnetization, and permeability measurements were performed on the ferromagnetic Heusler alloys $Ni_{52}Mn_{12.5}Fe_{12.5}Ga_{23}$ and $Ni_2Mn_{0.75}Cu_{0.25}Ga$.

1.   Thermal expansion

When cooling from austenite phase, steep decrease due to the martensitic transformation was obtained for both alloys. T_M and T_R increase gradually with increasing magnetic fields.

The shifts of T_M for Ni$_{52}$Mn$_{12.5}$Fe$_{12.5}$Ga$_{23}$ and Ni$_2$Mn$_{0.75}$Cu$_{0.25}$Ga in magnetic fields were estimated as dT_M/dB ≈ 0.5 K/T and 1.2 T/K, respectively.

2.   Magnetization and permeability

Ni$_{52}$Mn$_{12.5}$Fe$_{12.5}$Ga$_{23}$ ---- The M-B curves indicate that the property of the Ferro-M phase is different from the Ferro-A phase. The Ferro-A phase is considered to be a more localized ferromagnetic phase as compared with Ferro-M phase.

Ni$_2$Mn$_{0.75}$Cu$_{0.25}$Ga ---- The permeability abruptly changes around T_M. The permeability below T_M is about one-tenth times higher than that above T_M. The Arrott plot of magnetization indicates that T_C of the martensite phase is 307 K, which is almost the same as T_M = 308 K.

3.   The values of dT_M/dB are roughly proportional to the change of the spontaneous magnetization (M_M -M_A)/M_M. T_M of the ferromagnetic Heusler alloys Ni$_{52}$Mn$_{12.5}$Fe$_{12.5}$Ga$_{23}$ and Ni$_2$Mn$_{0.75}$Cu$_{0.25}$Ga in the magnetic field is considered to be shifted in accordance with the magnetic fields and proportional to the difference between the magnetization of austenite phase with that of martensite phase.

Ni$_2$MnGa$_{0.88}$Cu$_{0.12}$

Thermal expansion, permeability, magnetization measurements were performed on the Heusler alloy Ni$_2$MnGa$_{0.88}$Cu$_{0.12}$.

1.   Thermal expansion

When cooling from austenite phase, a steep decrease due to the martensitic transition was obtained. T_M and T_R increase gradually with increasing magnetic fields. The shift of T_M was estimated as dT_M/dB = 1.3 K/T.

2.   Magnetization and permeability

The permeability abruptly changes and shows the clear peak around T_M. The permeability below T_M is about one-tenth than that above T_M. The temperature dependence of the magnetization also shows a clear decrease around T_M. The Arrott plot of magnetization indicates that T_C of the martensite phase is 340 K, which is almost the same as T_M = 337 K, which was obtained by the linear expansion.

3.   The values of dT_M/dB are roughly proportional to the change of the spontaneous magnetization (M_M -M_A)/M_M in Ni$_2$MnGa type Heusler alloys. T_M of the ferromagnetic Heusler alloy Ni$_2$MnGa$_{0.88}$Cu$_{0.12}$ in the magnetic field is considered to be shifted in accordance with the magnetic fields and proportional to the difference between the magnetization of austenite and martensite phase.

Ni$_{52}$Mn$_{25}$Ga$_{23}$

Thermal strain, permeability, and magnetization measurements were performed on the Heusler alloy Ni$_{52}$Mn$_{25}$Ga$_{23}$.

1. Thermal strain: When cooling from the austenite phase, a steep decrease in the thermal strain is obtained because of the martensite transition. T_M and T_R increase gradually with increasing magnetic fields. The shifts in T_M and T_R in a magnetic field are estimated as $dT_M/dB = 0.46$ K/T and $dT_R/dB = 0.43$ K/T, respectively.

2. Magnetization and permeability: Permeability abruptly changes around T_M and T_R. Permeability below T_M is about one-third that above T_M. The temperature dependence of the magnetization also shows a clear discontinuity around T_M. The Arrott plot of magnetization indicates that T_C is 358 K. The sudden decrease in magnetization at the temperature of the martensite transition and the M–B curve indicate the magnetism of the hard Ferro–M phase and the soft Ferro–A phase.

3. The dT_M/dB values are roughly proportional to the change in spontaneous magnetization $[(M_M - M_A)/M_M]$ in Ni_2MnGa-type Heusler alloys. The T_M of the ferromagnetic Heusler alloy $Ni_{52}Mn_{25}Ga_{23}$ in the magnetic field is considered to be shifted in accordance with the magnetic fields and proportional to the difference in magnetization between the austenite and martensite phases.

Author details

T. Sakon[*]
Department of Mechanical System Engineering, Faculty of Science and Technology, Ryukoku University, Japan
Department of Mechanical Engineering, Graduate School of Engineering and Resource Science, Akita University, Japan

H. Nagashio, K. Sasaki, S. Susuga, D. Numakura and M. Abe
Department of Mechanical Engineering, Graduate School of Engineering and Resource Science, Akita University, Japan

K. Endo, S. Yamashita and T. Kanomata
Faculty of Engineering, Tohoku Gakuin University, Japan

H. Nojiri
Institute for Materials Research, Tohoku University, Japan

Acknowledgement

[*] Corresponding Author

5. References

[1] K. Ullakko, J.K. Huang, C. Kantner, R.C. O'Handley, V.V. Kokorin, *Appl. Phys. Lett.* 69 (1996) 1966.

[2] P.J. Webster, K.R.A. Ziebeck, S.L. Town, M.S. Peak, *Philos. Mag. B* 49 (1984) 295.

[3] P.J. Brown, J. Crangle, T. Kanomata, M. Matsumoto, K-.U. Neumann, B. Ouladdiaf, K.R. A. Ziebeck, *J. Phys: Condens. Matter* 14 (2002) 10159.

[4] J. Pons, R. Santamarta, V.A. Chernenko, E. Cesari, *J. Appl. Phys.* 97 (2005) 083516.

[5] R. Ranjan, S. Banik, S.R. Barman, U. Kumar, P.K. Mukhopadhyay, D. Pandey, *Phys. Rev. B* 74 (2006) 224443.

[6] C. Jiang, G. Feng, S. Gong, H. Xu, *Mater. Sci. Eng. A*, 342 (2003) 231.

[7] Y. Ma, C. Jiang, Y. Li, H. Xu, C. Wang, X. Liu, *Acta. Mater.* 55 (2007) 1533.

[8] L. Manosa, X. Moya, A. Planes, T. Krenke, M. Acet, E.F. Wassermann, *Mater. Sci. Eng. A* 481–482 (2008) 49.

[9] V. Sanchez-Ala'rcos J.I. Perez-Landaza'bal, C. Go'mez-Polo, V. Recarte, *J. Magn. Magn. Mater.* 320 (2008) e160.

[10] A. Rudajevov´a, *J. Alloys Compd.* 430 (2007) 153.

[11] F.Q. Zhu, F.Y. Yang, C.L. Chien, L. Ritchie, G. Xiao, G.H. Wu, *J. Magn. and Magn. Mater.* 288 (2005) 79.

[12] V.A. Chernenko, V.A. L'vov, V.V. Khovailo, T. Takagi, T. Kanomata, T. Suzuki, R. Kainuma, *J. Phys.: Condens. Matter* 16 (2004) 8345.

[13] V.O. Golub, A.Y. Vovk, C.J. O'Connor, V.V. Kotov, P.G. Yakovenko, K. Ullakko, *J. App. Phys.* 93 (2003) 8504.

[14] J. Kim, F. Inaba, T. Fukuda, T. Kakeshita, Acta Materialia 54 (2006) 493.

[15] A. Gonzalez-Comas, E. Obrado, L. Mafiosa, A. Planes, A. Labarta, *J. Magn. Magn. Mater.* 196-197 (1999) 637.

[16] N. Lanska, O. So¨derberg, A. Sozinov, Y. Ge, K. Ullakko, V.K. Lindroos, *J. App. Phys.* 95 (2004) 8074.

[17] A.A. Likhachev, K. Ullakko, *Phy. Lett. A* 275 (2000) 142.

[18] S.J. Murray M. Farinelli, C. Kantner, J.K. Huang, S.M. Allen, R.C. O'Handley, J. App. Phys. 83 (1998) 7297.

[19] K. Endo, T. Kanomata, A. Kimura, M. Kataoka, H. Nishihara, R. Y. Umetsu, K. Obara, T. Shishido, M. Nagasako, R. Kainuma, K. R. A. Ziebeck, edited by V.A. Chernenko, *Materials Science Forum* 684 (2011) 165.

[20] D. Kikuchi, T. Kanomata, Y. Yamauchi, H. Nishihara: *J. Alloys Compounds* 426 (2006) 223.

[21] A. N. Vasil'ev, E. I. Estrin, V. V. Khobailo, A. D. Bozhko, R. A. Ischuk, M. Matsumoto, T. Takagi, J. Tani: *Int. Appl. Electromagn. Mechan.* 12 (2000) 35.

[22] D. Kikuchi, Thesis, Tohoku-Gakuin Univ. 2010.

[23] M. Kataoka, K. Endo, N. Kudo, T. Kanomata, H. Nishihara, T. Shishido, R.Y. Umetsu, N. Nagasako, R. Kainuma: *Phys. Rev. B* 82 (2010) 214423.

[24] C. Kittel, *Introduction to Solid State Physics* (John Wiley & Sons, NJ, USA, 2005) 8th ed., p 75.

[25] P. Entel, V. D. Buchelnikov, V. V. Khovalio, A. T. Zayak, W. A. Adeagbo, M. E. Gruner, H. C. Herper, E. F. Wassermann: *J. Phys, D: Appl. Phys.* 39 (2006) 865-889.

[26] Bozorth R M 1951 *Ferromagnetism* p. 32 (D. van Nostrand)

[27] T. Sakon, H. Nagashio, K. Sasaki, S. Susuga, K. Endo, H. Nojiri, T. Kanomata, *Mater. Trans.* 52 (2011) 1142.

[28] A. N. Vasil'ev, E. I. Estrin, V. V. Khovailo, A. D. Bozhko, R. A. Ischuk, M. Matsumoto, T. Takagi, J. Tani, *Int. Appl. Electromagn. Mechan.* 12 (2000) 35.

[29] D. Kikuchi, T. Kanomata, Y. Yamaguchi, H. Nishihara, *J. Alloys Compd.* 426 (2006) 223.

[30] A.N. Vasil'ev, E.I. Estrin, V.V. Khovailo, A.D. Bozhko, R.A. Ischuk, M. Matsumoto, T. Takagi, J. Tani, *Int. J. Appl. Electromagn. Mechan.* 12 (2000) 35.

[31] L. Dai, J. Cullen, M. Witting, *J. Appl. Phys.* 95 (2004) 6957.

[32] R.Z. Levitin, V.V. Snegirev, A.V. Kopylov, A.S. Lagutin, A. Gerber, *J. Magn. Magn. Mater.* 170 (1997) 223.

[33] J. Markos, A. Planes, L. Manosa, F. Casanova, X. Battle, A. Labarta, B. Martinez, *Phys. Rev. B* 66 (2002) 224413.

[34] T. Krenke, M. Acet, E. F. Wassermann, X. Moya, L. Manosa, A. Planes, *Phys. Rev. B* 72 (2005) 014412.

[35] A.Gonzàlez-Comas, E. Obradó, L. Mãnos, A. Planes, V.A. Chernenko, B.J. Hattink, A. Labarta, *Phys. Rev. B* 60 (1999) 7085.

[36] D.A. Filippov, V.V. Khovailo, V.V. Koledov, E.P. Krasnoperov, R.Z. Levitin, V.G. Shavrov, T. Takagi, *J. Magn. Magn. Mater.* 258–259 (2003) 507.

[37] V.V. Khovailo, V. Novosad, T. Takagi, D.A. Filippov, R.Z. Levitin, A.N. Vasil'ev, *Phys. Rev. B* 70 (2004) 174413.

[38] V.V. Khovailo, T. Takagi, T.J. Tani, R.Z. Levitin, A.A. Cherechukin, M. Matsumoto, R. Note, *Phys. Rev. B* 65 (2002) 092410.

[39] T. Sakon, H. Nagashio, K. Sasaki, S. Susuga, D. Numakura, M. Abe, K. Endo, H. Nojiri, T. Kanomata, *Physica Scripta* 84 (2011) 045603.

[40] S. Aksoy, T. Krenke, M. Acet, E. F. Wassermann, *Appl. Phys. Lett.* 91 (2007) 251915.